SEL-65-102

INTERPRETATION OF IMPEDANCE PROBE MEASUREMENTS IN THE IONOSPHERE

by

R. J. L. Grard

December 1965

Technical Report No. 2

Prepared under
National Aeronautics and Space Administration
Grant No. NsG 174-61

Radioscience Laboratory
Stanford University Stanford, California

26656

ABSTRACT

Measurements of the very low frequency impedance of the sheath which surrounds a probe in the ionosphere can provide instantaneous and continuous information on the electron density and temperature.

A simplified theory of the sheath was developed and its validity was checked in the laboratory. Variations of the sheath impedance with frequency, electron density and probe potential are presented.

The ac impedance of a dipole was measured in the ionosphere. The interpretation of the data is complicated by the effect of the earth's magnetic field and the wake of the rocket, but the theoretical treatment is shown to apply with reasonable accuracy at low frequency.

We conclude with a discussion of the utility of impedance measurements in the ionosphere as a diagnostic technique.

CONTENTS

TABLES

ILLUSTRATIONS

ACKNOWLEDGMENT

I am very grateful to Professor Robert A. Helliwell and Dr. F. W. Crawford for their numerous suggestions and constant encouragement. I wish to thank Professors W. R. Rambo and O. K. Garriott for their help as well as Drs. R. L. Smith and D. L. Carpenter. I acknowledge the work of Messrs. L. E. Orsak, G. B. Carpenter, B. P. Ficklin and L. H. Rorden concerning the reduction and interpretation of the ionospheric data. I am also indebted to the late Dr. R. F. Mlodnosky, who suggested this research.

The work presented here was sponsored by the National Aeronautics and Space Administration under Grant NsG 174-61. The author is grateful for subsistence support provided by the Alliance Francaise de New York, the Organisation du Traité de l'Atlantique Nord, and the Organisation de Coopération et de Developpement Economiques.

I. INTRODUCTION

The determination of the parameters of the ionized gas which lies in the upper atmosphere is important for many reasons. For example, this natural plasma profoundly affects the propagation of radio waves over a wide range of frequencies. Also it plays an important role in various natural phenomena such as very low frequency emissions, the aurorae and magnetic storms.

The most important of these parameters, the electron density, was first measured by its effect upon the propagation of an electromagnetic wave. The vertical sounding method, described by Breit and Tuve,[1] measures the time required by a short electromagnetic signal, transmitted from the ground, to come back after being reflected by the ionosphere. The electron density can be plotted against the altitude by varying the frequency of the carrier, but this method does not allow one to record the electron density profile at an altitude higher than the point of maximum electron concentration.

Propagation measurements with rockets were initiated by Seddon.[2] In these experiments one obtains the electron density from the frequency shift of a wave which has traveled from the rocket to the ground.

The phenomenon of Faraday rotation can also be utilized in the determination of ionospheric parameters. One measures the rotation of the polarization plane of a transverse linearly polarized wave propagating in a magnetoplasma. This technique and all propagation experiments in general yield a measure of the electron density integrated over the path of the wave and tend to smooth away the irregularities of the electron density profile of small size with respect to the wavelength.

In order to get better resolution in altitude it seems advantageous to use a probe carried by a rocket or a satellite and to measure the characteristics of the probe which are functions of the local parameters of the plasma.

Following this line one may apply to the ionosphere the method designed for the laboratory by Langmuir and Mott-Smith.[3] Assuming that the electron velocity distribution function is Maxwellian, one can

determine the electron density and temperature by plotting the dc volt-ampere characteristic of the probe. Predictions for the dc characteristic of an ionospheric dumbbell probe were made by Hoegy and Brace.[4] The Langmuir technique requires the location of the space potential on the probe characteristic. This operation is delicate in the laboratory and can be hazardous in the more complicated conditions of the ionosphere. A more sophisticated device, the pulse probe, was proposed by Bettinger;[5] this method does not assume a priori a Maxwellian distribution function for the electron velocity, but is more complicated experimentally. Schematically the pulse probe consists of an inner collector held at a fixed potential and surrounded by a screen cage. All electrons in the interior of the cage are driven to the collector when a negative pulse is applied to the cage. Knowledge of the collected current, the cage volume and the pulse repetition frequency yields the electron density at the probe surface.

Takayama, Ikegami and Miyasaki[6] made an original approach to this problem with the resonance probe. They showed that, if a constant potential in series with an rf signal is applied to a probe, one could determine the electron temperature and the plasma frequency by recording the dc current flowing to the probe as a function of the frequency of the alternating signal. It was shown by Harp and Crawford[7] and Fejer[8] that the resonance does not occur exactly at the plasma frequency, but provided the form of the expression for resonance is known, this probe can provide a useful diagnostic technique without much complication.

A different method consists of measuring the impedance between two probes or between one probe and the body of the rocket or satellite, as shown on Fig. 1. According to the geometry of the system and the working frequency, this technique can be divided roughly into two classes. With the first kind, which we will call "plasma impedance probe," one determines the local permittivity of the ionosphere by measuring the impedance of the system with the plasma as a dielectric. The perturbation due to the positive sheath which surrounds the electrodes and the effects of the plasma temperature are neglected. Detailed

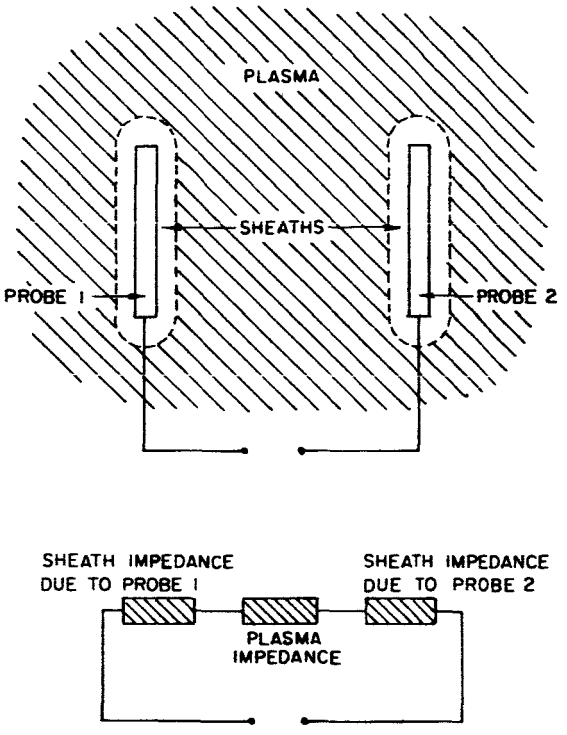

FIG. 1. A SKETCH OF THE IMPEDANCE PROBE AND THE EQUIVALENT CIRCUIT SHOWING THE COMPONENTS OF THE IMPEDANCE.

treatments of the impedance of a dipole in a magnetoplasma were made by Balmain[9] and Blair.[10] Ionospheric experiments were realized by Kane, Jackson and Whale[11] and Crouse.[12] This method yields the electron density and, possibly, the collision frequency.

The second kind of technique is generally used at much lower frequency. We will call it "sheath impedance probe" because it is then possible to make the opposite approximation; the impedance of the system is due mainly to the ion sheath and the effect of the plasma is neglected. Mlodnosky and Garriott[13] suggested that this technique could yield the electron density, the electron temperature and the space potential. They predicted the value of the admittance of the positively charged sheath which forms around the probe. The sheath incremental conductance is the slope of the dc volt-ampere characteristic. They computed the capacitance of the probe, assuming that the sheath was sharply bounded and empty of electrons. This model was modified by Grard[14] who, applying Boltzmann's law to the electron density in the sheath, derived the sheath capacitance from Poisson's equation. Similar modifications and a

discussion of the limitations of this method were made by Crawford and Mlodnosky.[15]

Compared to the propagation methods, the probe techniques offer high spatial resolution, although their resolving power is not limited by their size, but by the distance traveled by the carrying vehicle, rocket or satellite, during the time required to make one measurement. The common inconveniences of the probes are due mainly to the fact that they perturb the medium in which they are moving. The trail left behind a satellite was studied by Jastrow and Pearse,[16] and Al'pert, Gurevich and Pitaevskiĭ,[17] who showed that the wake is important when the velocity of the body is larger than the thermal velocity of the particles. Photoemission is another source of error, and the presence of the earth's magnetic field complicates the computation of the plasma impedance and perturbs the motion of the particles in the sheath.

The present work deals mainly with the sheath impedance probe; that is, the impedance probe in the very low frequency approximation, where the ion sheath is responsible for the impedance of the probe.

The study which is presented in the following chapters has been motivated by several reasons. First, there is a need for new ionospheric diagnostic methods which can match the present requirements of space research. It had been suggested by Mlodnosky and Garriott[13] that the electron temperature and density could be determined from the measurements of the sheath impedance, but it was necessary to improve their theoretical model and test its validity; it was important to show the advantages of this method but also to point out its faults and limitations. Secondly, there were available a set of unique vlf impedance probe measurements made in the ionosphere by Orsak, Rorden, Carpenter, and Ficklin,[18] but it was necessary to improve our understanding of the sheath phenomenon before giving an interpretation of these data. Finally, independent of the applications of the sheath properties as a diagnostic method, an improvement of the sheath theory was very important for the accurate determination of the impedance of any antenna in a plasma. Effectively, the depletion of electrons in the vicinity of an antenna changes its impedance and may perturb its receiving and transmitting characteristics.

This report is divided into three chapters. In Chapter II we present a simplified theory of the sheath. First, we review briefly Bohm's[19] theory about the determination of the floating potential, because we will use it later on for numerical comparison. Then we present the model given by Mlodnosky and Garriott[13] for the conductance of the sheath, which is fairly satisfactory. Finally, we present several models for the sheath capacitance which are all original but one, borrowed from Butler and Kino.[20] The models considered fall into two classifications. In the first group, we do not take into consideration the ac motion of the ions and the treatment is valid at relatively high frequency where the ions cannot follow the variations of the ac electric field applied to the probe. With one model, we consider a smooth variation of the electron density from the sheath to the undisturbed plasma, rather than a step transition. In the two other models we take into consideration the rarefaction of the ion density due to ion acceleration by the dc electric field of the sheath. It is interesting to note that all the preceding models give very similar results in spite of the differences between the initial assumptions. In the second class of models, the variation of the ion density with the ac applied electric field is also taken into account. This representation, which is valid in the lower frequency range, is found to give answers differing from those found from the three first models.

In order to check the validity and the range of applicability of the formulas derived in Chapter II under known and controllable conditions, a laboratory experiment was set up to measure the sheath admittance. A special tube was designed for this purpose and for the first time we made ac measurements of the sheath impedance and interpreted them. Typical results of this experimentation are shown in Chapter III. We present unique data on the variations of the sheath admittance with frequency, electron density and probe potential. These laboratory measurements are important because they are the only reliable tests of the validity of the theoretical treatment of the sheath; furthermore, they suggest diagnostic methods in the laboratory which have never been used before. The laboratory results are extremely valuable not only

for the interpretation of the ionospheric data but also for the design of a new space experiment.

Chapter IV deals with the interpretation of ionospheric vlf impedance probe measurements made by Orsak et al.[18] The ac impedance of a dipole was measured in the ionosphere at frequencies of 1.54 kc/s and 120 kc/s. The 1.54 kc/s data are considered representative of the sheath, because it may be shown that the impedance of the plasma is negligible at that frequency.

The 120 kc/s results are not considered to characterize the sheath, because the plasma beyond the sheath is believed to modify the measured impedance. It was not possible to take its effect into consideration, however, because Poisson's equation is hyperbolic at that frequency in the conditions of the rocket flight. No reliable theory allows us to compute at present the impedance of an antenna in a uniform magnetoplasma under hyperbolic conditions, and we point out that there is a need for more experimental data in this field. We suggest that complications may arise at low frequency in the computation of the impedance of a dipole when the distance traveled by the particles during one period of the applied electric field becomes comparable to the size of the antenna. Kaiser[21] had also suggested that, in such conditions, the cold plasma theory was no longer valid. We support this statement by computing this temperature effect on the capacitance of a planar condenser for two different kinds of velocity distribution function. The effect of a magnetic field is also considered. This study warns us that the cold plasma approximation can be misleading at low frequencies.

Finally, in our conclusions, we discuss the utility of the vlf impedance probe in the ionosphere. We present the possibilities and limitations of this technique and we use the experience gained through laboratory measurements and interpretation of ionospheric data to show how this probe can be improved and how we can increase our knowledge of the sheath.

II. THEORY OF THE VLF ADMITTANCE PROBE

A. FORMATION AND DESCRIPTION OF THE POSITIVE SHEATH

In a plasma the electron velocity is generally much higher than the ion velocity. If the different species of particles are in thermal equilibrium, the velocity of a given particle is inversely proportional to the square root of its mass. For example, the ratio of the electron thermal velocity over the ion thermal velocity equals 43 for a plasma made of ionized atomic hydrogen.

Consequently, when an uncharged probe is immersed in a plasma, it collects more electrons than ions during a transient period and becomes more and more negatively charged up to the point where its potential with respect to the neutral plasma is sufficiently negative to limit the flow of electrons. An equilibrium regime is reached when the flow of electrons equals the flow of ions.

Only those electrons which have a velocity component normal to the surface of the probe high enough to overcome the negative potential can be collected. The others are reflected at a distance from the probe which depends on their normal velocity.

Therefore there is a relatively low density of electrons in the immediate vicinity of the probe. This region is positively charged and is called the sheath. The charge of the sheath is equal in magnitude and opposite in sign to the charge carried by the probe, since the medium must remain neutral from a macroscopic point of view.

B. THE FLOATING POTENTIAL OF THE PROBE

The negative equilibrium of the probe, or floating potential, has been computed by Bohm et al[19] for a planar geometry, and we shall review briefly his theory. Let us assume that the singly charged ions arrive at the sheath edge with a velocity perpendicular to the probe surface and an energy which, measured in electron volts, equals eV_i. The ions are accelerated in the sheath and, from the continuity equation and energy conservation, we find that their density is given by

$$n_i = n\sqrt{\frac{V_i}{V_i - V}} , \qquad (1)$$

where n is the ion or electron density in the unperturbed plasma and V is the potential in the sheath with respect to the neutral plasma. Assume the electron distribution function to be Maxwellian, i.e., given by

$$f(v) = \frac{1}{v_o\sqrt{\pi}} \exp\left(-\frac{v^2}{v_o^2}\right) ,$$

where v_o is the thermal velocity of the particles, and v is the component of the electron velocity normal to the probe. If the probe is a perfect reflector, we can apply Boltzmann's law to the electron density in the sheath and write

$$n_e = n \exp\frac{V}{V_e} , \qquad (2)$$

where V_e, the electron potential, equals $\frac{1}{2}\frac{m}{e}v_o^2$, m and e being respectively the mass and charge of an electron.

However, a metallic probe should instead be considered as being a perfect collector. The electrons which have a normal velocity in the sheath such that

$$\frac{1}{2}mv^2 > e(V-V_o) ,$$

V_o being the potential of the probe with respect to the neutral plasma, reach the probe. Therefore they are collected and are missing from the velocity distribution function, as shown on Fig. 2. The electron density becomes

$$n_e = n \exp\frac{V}{V_e}\frac{1}{v_o\sqrt{\pi}}\left[\int_{-\infty}^{o} \exp\left(-\frac{v^2}{v_o^2}\right)dv + \int_{o}^{\sqrt{\frac{2e}{m}(V-V_o)}} \exp\left(-\frac{v^2}{v_o^2}\right)dv\right] ,$$

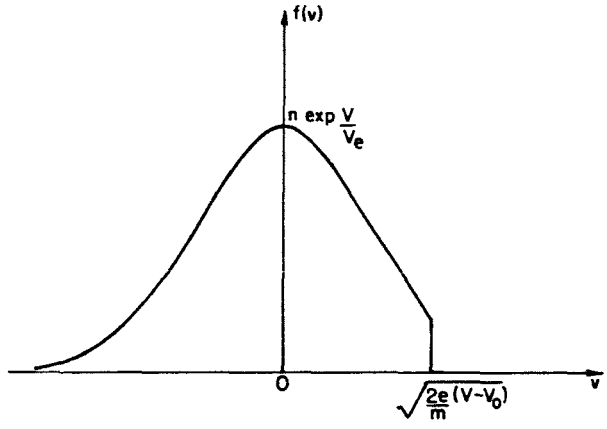

FIG. 2. ELECTRON VELOCITY DISTRIBUTION IN THE SHEATH.

$$n_e = \frac{n}{2} \exp \frac{V}{V_e} \left(1 + \operatorname{erf} \sqrt{\frac{V-V_o}{V_e}} \right). \qquad (3)$$

The magnitude of the error made in the determination of the electron density by Eq. (2) is maximum at the surface of the probe, but, when $|V_o| > 2.3\ V_e$, it never exceeds 5 percent of the unperturbed electron density. It is then a good approximation to use Boltzmann's law when the potential of the probe is very negative.

Furthermore, use of Eq. (3) introduces an inconsistency because the electron density in the unperturbed plasma, where $V = 0$, becomes

$$n_e = \frac{n}{2} \left(1 + \operatorname{erf} \sqrt{-\frac{V_o}{V_e}} \right)$$

instead of n, and varies with the probe potential.

In practice, an electrode has a finite size and this incompatibility does not exist because the full Maxwellian electron velocity distribution function is restored at infinity.

Consequently, substituting Eqs. (1) and (2) in Poisson's equation, one obtains

$$\frac{\partial^2 V}{\partial r^2} = - \frac{ne}{\epsilon_o} \left(\sqrt{\frac{V_i}{V_i - V}} - \exp \frac{V}{V_e} \right), \qquad (4)$$

where ϵ_o is the vacuum dielectric constant.

Integrated once, this equation becomes

$$\left(\frac{\partial V}{\partial r}\right)^2 = \frac{2ne}{\epsilon_o}\left(2\sqrt{V_i(V_i-V)} + V_e \exp\frac{V}{V_e}\right) + K \ ,$$

where K is found from the boundary condition at the sheath edge, $V = \partial V/\partial r = 0$. Replacing for K we find

$$\left(\frac{\partial V}{\partial r}\right)^2 = \frac{2ne}{\epsilon_o}\left[2\sqrt{V_i(V_i-V)} - 2V_i - V_e\left(1 - \exp\frac{V}{V_e}\right)\right]. \qquad (5)$$

Expanding for small value of V in a region close to the sheath edge we obtain

$$\left(\frac{\partial V}{\partial r}\right)^2 = \frac{ne}{\epsilon_o}\left(\frac{1}{V_e} - \frac{1}{2V_i}\right)V^2$$

We see that $(\partial V/\partial r)^2$ is positive only if $V_e/V_i < 2$ and, following Bohm, we can say that the sheath edge is located where $V_i = V_e/2$.

We can use this result to compute the floating potential of the probe. The ion current at the sheath edge is written

$$I_p = Ane\sqrt{\frac{2eV_i}{M}} = Ane\sqrt{\frac{eV_e}{M}} \ ,$$

where M is the ion mass and A is the area of the probe.

On the other hand the random electron current collected by the probe can be shown to be

$$I_e = Ane\sqrt{\frac{eV_e}{2\pi m}} \exp\frac{V_o}{V_e} \ . \qquad (6)$$

At floating potential, V_f, the total current collected by the probe is zero, then

$$I_p = I_e \tag{7}$$

and

$$V_f = -\frac{V_e}{2} \ln \frac{M}{2\pi m} \tag{8}$$

This formula gives $V_f = -5.49\ V_e$ for mercury, $V_f = -4.23\ V_e$ for oxygen and $V_f = -2.84\ V_e$ for hydrogen.

A more accurate theory of the probe potential would require a more refined computation of the ratio V_e/V_i at the sheath edge, taking into account the generation of ions in the plasma. This probem was considered by Self[22] in planar geometry and by Parker[23] in cylindrical geometry. We shall note that, since V_f varies like the logarithm of V_e/V_i, the accuracy of the determination of this ratio is not critical.

C. THE AC CONDUCTANCE OF THE SHEATH

We will summarize here the treatment given by Mlodnosky and Garriott[13]. The dc current collected by a probe is given by the difference between the electron and ion flows,

$$I = I_p - I_e \ .$$

There is no straightforward way of writing an expression for the ion current as a function of the potential, but the electron current, which is not a function of the probe geometry, is given by Eq. (6) and can be written

$$I_e = I_{se} \exp \frac{V_o}{V_e} \ ,$$

assuming that the velocity distribution function is Maxwellian and that the potential of the probe with respect to the space potential is negative. I_{se}, the saturation current, or electron random current collected by the probe at space potential, is given by

$$I_{se} = Ane\sqrt{\frac{eV_e}{2\pi m}} , \tag{9}$$

The ac conductance of the sheath equals the derivative of the current with respect to potential

$$G_s = \frac{\partial I_p}{\partial V_o} + \frac{I_{se}}{V_e} \exp \frac{V_o}{V_e} .$$

If the variations of the ion current with potential can be neglected, we reach the simplified result

$$G_s = \frac{I_{se}}{V_e} \exp \frac{V_o}{V_e} = \frac{I_e}{V_e} . \tag{10}$$

From the measurement of the sheath conductance of the probe at floating potential it seems that we could determine the saturation current

$$I_{se} = G_s V_e \exp \left(- \frac{V_f}{V_e} \right)$$

and then compute the electron density from Eq. (9), assuming that V_f and V_e are known. This would be an awkward approach because I_{se} varies exponentially with V_f and the slightest error made in the measurement of V_f would have the worst consequences in the computation of I_{se}. Moreover, the electrons which are collected by the negative probe are the most energetic and belong to the tail of the velocity distribution function. A Maxwellian function is a suitable description of the velocity distribution function of electrons with an energy less than about $4eV_e$, but is not always a valid representation of the tail of the distribution.

On the other hand it would be convenient to make the maximum use of the conductance measurements because, unlike the sheath capacitance, the conductance is not a function of the probe geometry.

If the probe potential is increased but kept less than the space potential, electrons of lower energy are collected and their velocity distribution function is more closely represented by a Maxwellian function. Then, if we measure the conductance and the dc current of the probe we can determine the electron temperature, $V_e = G_s/I_e$, with fair accuracy.

Knowing V_e and assuming that we can get the electron density from the capacitance measurement, we compute the saturation current and reach the floating potential through the relation

$$V_f = - V_e \ \ell n \frac{I_{se}}{G_s V_e}.$$

One notes that a lack of accuracy in the determination of I_{se}/G_s does not perturb seriously the value of V_f. Then one can check if this value of V_f is consistent with that adopted in the capacitance computation.

D. THE AC CAPACITANCE OF THE SHEATH

1. Definition of the Sheath Capacitance

When one adds to the negative potential of the probe, V_o, some positive increment ΔV_o with respect to the potential of the plasma at infinity, the sheath becomes thinner and its positive charge, Q_o, decreases by a corresponding quantity ΔQ_o. In order for the medium to remain neutral, the negative charge borne by the probe must algebraically increase by the same amount. Therefore the ratio $\Delta Q_o/\Delta V_o$ is positive.

We define the incremental, or dynamic, capacitance as being the partial derivative of the charge carried by the probe with respect to its potential, $C_s = \partial Q_o/\partial V_o$.

We will give several expressions of the sheath capacitance for a plane surface in rectangular coordinates, a cylinder of revolution in cylindrical coordinates, and a sphere in spherical coordinates (Fig. 3). We assume respectively planar, cylindrical or spherical

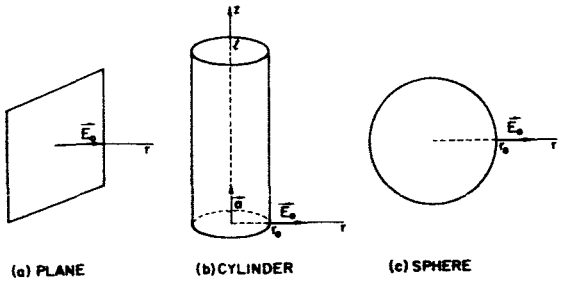

FIG. 3. DIFFERENT PROBE GEOMETRIES.

symmetry for the electric quantities on the surface and in the vicinity of these conductors. We neglect the edge effect on the borders of the plane and at the tips of the cylinder. The edge effect is negligible if the thickness of the sheath is much smaller than the size of the probe. In a practical case it is possible to minimize this perturbing effect by the use of a guard ring.

We are using two basic methods for computing the sheath capacitance. In the first method one estimates the thickness of the sheath and assumes that the electron density is unperturbed outside the sheath and zero inside. One also assumes that the ions are attracted by the negative dc potential of the probe but that their velocity is not modulated by the superimposed ac potential. Then the permittivity of the sheath is that of vacuum and the capacitance is that of two parallel electrodes, or coaxial cylinders, or concentric spheres, separated by a distance equal to the sheath thickness.

In the second method one computes the electric field at the surface of the probe and, using Gauss' theorem, writes that the charge borne by the probe is

$$Q_o = A \epsilon_o E_o ,$$

where E_o is the electric field at the surface.

By definition the electric field in the medium surrounding the probe is $E = -\nabla V$; because of the symmetry in each case we have $\nabla V = \partial V/\partial r$.

Consequently, $E_o = - (\partial V/\partial r)_o$, where $(\partial V/\partial r)_o$ is the value of $\partial V/\partial r$ on the surface of the probe.

Then the expression for the capacitance becomes

$$C_s = - A \epsilon_o \frac{\partial}{\partial V_o} \left(\frac{\partial V}{\partial r} \right)_o . \tag{11}$$

Now, it is convenient to define a new set of variables:

$$y = \frac{V}{V_e}$$

and

$$x = \frac{r}{\lambda_D} ,$$

where $\lambda_D = \sqrt{\frac{\epsilon_o V_e}{ne}}$ is the Debye length.

Using these dimensionless variables in the expression for the capacitance we write:

$$C_s = - A \frac{\epsilon_o}{\lambda_D} \frac{\partial}{\partial y_o} \left(\frac{\partial y}{\partial x} \right)_o ,$$

where $y_o = \frac{V_o}{V_e}$.

If, furthermore, we define a third dimensionless quantity,

$$\gamma = \frac{C_s}{A} \frac{\lambda_D}{\epsilon_o} , \tag{12}$$

which we will call normalized capacitance, we finally obtain

$$\gamma = - \frac{\partial}{\partial y_o} \left(\frac{\partial y}{\partial x} \right)_o . \tag{13}$$

One must note that the per unit area capacitance of an infinite plane or cylinder immersed in a plasma is well defined because the net charge of the probe surrounded by its sheath is zero and the probe potential remains finite. In free space, the problem is completely different because the potential of a charged body of infinite size is also infinite and the notion of capacitance is not useful.

2. Theoretical Determination of the Sheath Capacitance, Model I

a. Description of the Sheath Model

We assume that the electron velocity distribution function is Maxwellian and that we can apply Boltzmann's law to determine the electron density in the sheath. The validity of this assumption has been discussed previously. In a first approach we neglect the motion of the ions and consider that their density is unperturbed by the dc potential of the probe. Poisson's equation in the sheath is written

$$\nabla^2 V = -\frac{ne}{\epsilon_o}\left(1 - \exp\frac{V}{V_e}\right)$$

Expressing Poisson's equation in terms of y and x we have:

for a planar probe, $$\frac{\partial^2 y}{\partial x^2} = \exp y - 1, \qquad (14)$$

for a cylindrical probe, $$\frac{1}{x}\frac{\partial}{\partial x}\left(x\frac{\partial y}{\partial x}\right) = \exp y - 1, \qquad (15)$$

for a spherical probe, $$\frac{1}{x^2}\frac{\partial}{\partial x}\left(x^2\frac{\partial y}{\partial x}\right) = \exp y - 1 \ . \qquad (16)$$

b. Planar Geometry

Equation (14) is integrated once to give

$$\frac{\partial y}{\partial x} = \pm\sqrt{2(\exp y - y - K)} \ .$$

At $x = \infty$, y goes to zero and so does its derivative with respect to x, therefore the constant of integration K is evaluated to be 1 and

$$\frac{\partial y}{\partial x} = \pm\sqrt{2(\exp y - y - 1)} \ .$$

The value of $\partial y/\partial x$ on the surface is found by replacing y by y_o:

$$\left(\frac{\partial y}{\partial x}\right)_o = \pm\sqrt{2(\exp y_o - y_o - 1)} \quad .$$

Using Eq. (13), we finally obtain

$$\gamma = \pm \frac{\exp y_o - 1}{\sqrt{2(\exp y_o - y_o - 1)}} \quad .$$

Since y_o is negative and γ must be positive, we choose the minus sign in the above expression of γ. Having assumed that $|y_o|$ was large with respect to 1, we may neglect $\exp y_o$ with respect to 1 and write:

$$\gamma = [-2(y_o + 1)]^{-1/2} \tag{17}$$

Replacing for γ and y_o we obtain:

$$C_s = \epsilon_o \frac{A}{\lambda_D}\left[-2\left(\frac{V_o}{V_e} + 1\right)\right]^{-1/2} , \tag{18}$$

which is the capacitance of a planar sheath. We note that γ is the inverse of the equivalent sheath thickness measured in Debye length.

The normalized potential and electron density profiles, V/V_e and n_e/n respectively, were found from numerical integrations of Eq. (14) with a computer and are displayed on Fig. 4.

c. Cylindrical Geometry

In cylindrical coordinates Poisson's equation is given by Eq. (15).

We cannot integrate this differential equation as we did in rectangular coordinates. However, we assume that $\exp y$ may be neglected with respect to 1 within the sheath. In other words, we consider that

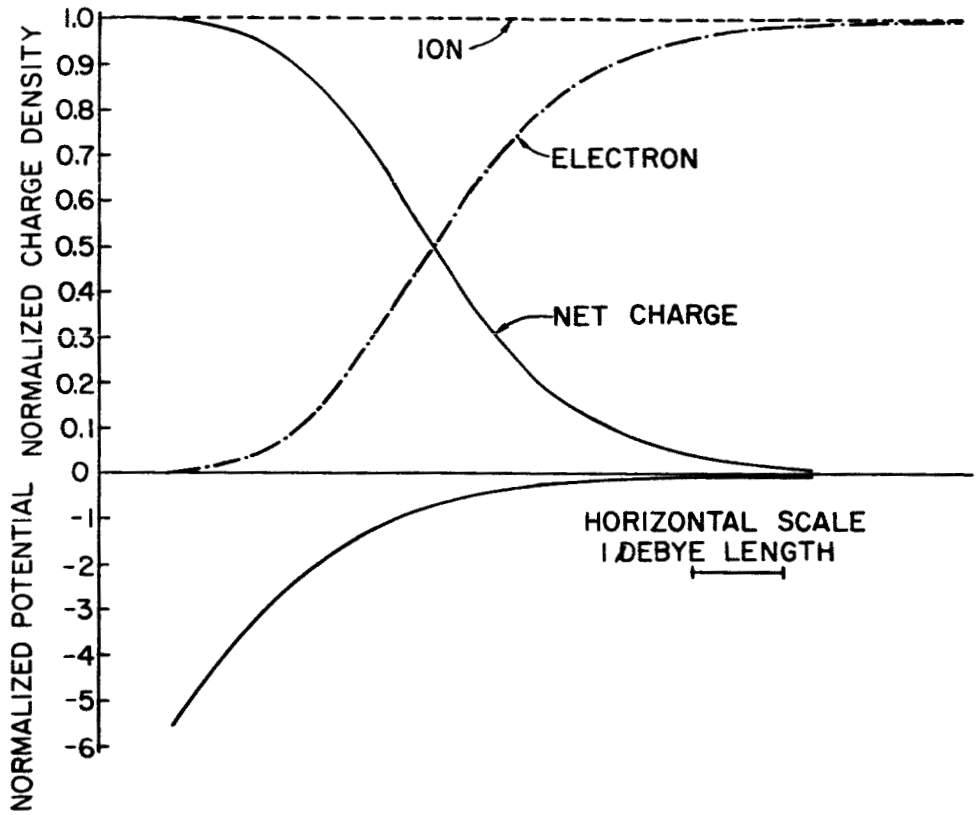

FIG. 4. CHARGE DENSITY AND POTENTIAL PROFILES IN THE SHEATH, MODEL I, PLANAR GEOMETRY.

the sheath is empty of electrons and sharply bounded. We define the radius of the probe r_o and the outer radius of the sheath r_1 and we put

$$x_o = \frac{r_o}{\lambda_D} \quad \text{and} \quad x_1 = \frac{r_1}{\lambda_D}$$

The simplified Poisson's equation becomes

$$\frac{1}{x} \frac{\partial}{\partial x} \left(x \frac{\partial y}{\partial x} \right) = -1$$

and its solution is

$$y = -\frac{x^2}{4} + K_1 \ln x + K_2 ,$$

where K_1 and K_2 are two constants of integration estimated from the boundary conditions at the sheath edge.

These conditions expressed in terms of y and x are:

$$\text{at} \quad x = x_1, \quad y = 0 \quad \text{and} \quad \partial y/\partial x = 0 \ .$$

They give:

$$K_1 = \frac{x_1^2}{2} \quad \text{and} \quad K_2 = \frac{x_1^2}{4} - \frac{x_1^2}{2} \ln x_1 \ .$$

We replace K_1 and K_2 in the above solution

$$y = \frac{1}{4}\left(x_1^2 - x^2\right) - \frac{x_1^2}{2} \ln \frac{x_1}{x} \ .$$

On the surface of the cylinder, at $x = x_o$, we obtain

$$y_o = \frac{1}{4}\left(x_1^2 - x_o^2\right) - \frac{x_1^2}{2} \ln \frac{x_1}{x_o}$$

and

$$\left(\frac{\partial y}{\partial x}\right)_o = - \frac{x_o}{2} + \frac{x_1^2}{2} \frac{1}{x_o} \ .$$

Equation (13) can also be written

$$\gamma = - \frac{\dfrac{\partial}{\partial x_1}\left(\dfrac{\partial y}{\partial x}\right)_o}{\dfrac{\partial y_o}{\partial x_1}}$$

with

$$\frac{\partial}{\partial x_1}\left(\frac{\partial y}{\partial x}\right)_o = \frac{x_1}{x_o} \quad \text{and} \quad \frac{\partial y_o}{\partial x_1} = - x_1 \ln \frac{x_1}{x_o} \ ,$$

that is

$$\gamma = \frac{1}{x_o \ln \frac{x_1}{x_o}} \quad .$$

Eliminating x_1 between y_o and γ, we reach an expression involving γ, y_o and x_o:

$$1 + \frac{4y_o}{x_o^2} = \left(1 - \frac{2}{\gamma x_o}\right) \exp \frac{2}{\gamma x_o} \qquad (19)$$

When x_o goes to infinity, Eq. (19) can be written

$$\gamma = (-2y_o)^{-1/2} \qquad (20)$$

which is the normalized capacitance of a planar and sharply bounded sheath. Comparing Eqs. (17) and (20) shows how γ is modified when one smoothes the charge density profile by applying Boltzmann's law to the electron density in the sheath.

d. Spherical Geometry

In spherical coordinates Poisson's equation is given by Eq. (16). We assume, as we did in cylindrical geometry, that the sheath is sharply bounded and that the radius of the probe and the radius of the sheath, measured in Debye lengths, are respectively x_o and x_1.

$$\frac{1}{x^2} \frac{\partial}{\partial x} \left(x^2 \frac{\partial y}{\partial x}\right) = -1$$

which, once integrated, gives

$$y = -\frac{x^2}{6} - \frac{x_1^3}{3x} + \frac{x_1^2}{2} \quad .$$

Following the same steps as before, we are able again to determine a relation between γ, y_o and x_o:

$$1 - 6\frac{\gamma}{x_o^2} = \frac{1 - \frac{2}{\gamma x_o}}{\left(1 - \frac{1}{\gamma x_o}\right)^3} \qquad (21)$$

Equation (21) also reduces to Eq. (20) when x_o goes to infinity.

3. Theoretical Determination of the Sheath Capacitance, Model II

a. Description of the Sheath Model

Our assumptions are basically the same as those made for Model I, but this time we will consider that the sheath is sharply bounded. Furthermore, we will assume that the ions are attracted by the dc potential of the probe and emitted at the sheath edge without initial velocity. Neglecting the presence of electrons in the sheath, the ion current is supposed to be limited by space charge like the electron current in a diode: the saturation regime determines the thickness of the sheath. The capacitance of the sheath is the same as the capacitance of the system formed by the probe and a conducting surface situated at the outer edge of the sheath. The space between these two surfaces has the permittivity of vacuum since the electronic charge in the sheath is negligible and the frequency of the alternating signal is supposed to be such that the ion current is negligible compared with displacement current.

b. Planar geometry

The ion current collected by the probe is given by the Child-Langmuir law

$$I_p = \frac{4}{9}\varepsilon_o A \left(\frac{2e}{M}\right)^{1/2} \frac{(-V_o)^{3/2}}{d^2}, \qquad (22)$$

where d is the thickness of the sheath.

Since the electron velocity distribution function is Maxwellian, the electron random current is given by Eq. (6). At floating potential Eq. (7) applies and

$$d = \frac{2}{3}\lambda_D \left(\frac{4\pi m}{M}\right)^{1/4} \left(-\frac{V_f}{V_e}\right)^{3/4} \exp\left(-\frac{V_f}{2V_e}\right).$$

The capacitance of the sheath, $C_s = \epsilon_o A/d$, becomes

$$C_s = \epsilon_o \frac{A}{\lambda_D} \frac{3}{2} \left(\frac{M}{4\pi m}\right)^{1/4} \left(-\frac{V_f}{V_e}\right)^{-3/4} \exp\frac{V_f}{2V_e} \qquad (23)$$

If we replace the ratio M/m in Eq. (23) by its value found from Eq. (8), we obtain

$$C_s = \epsilon_o \frac{A}{\lambda_D} \frac{3}{2} 2^{-1/4} \left(-\frac{V_f}{V_e}\right)^{-3/4} \qquad (24)$$

Comparing Eqs. (12) and (24) we finally reach the result

$$\gamma = \frac{3}{2} 2^{-1/4} (-y_f)^{-3/4} = 1.26\ (-y_f)^{-3/4}\ , \qquad (25)$$

where $y_f = V_f/V_e$.

The normalized potential is derived from Eq. (25) and is written

$$y = -1.365 \left(\frac{r}{\lambda_D}\right)^{4/3}$$

where the distance r is measured from the sheath edge toward the probe.

The normalized ion density in the sheath is given by

$$\frac{n_i}{n} = (-2y)^{-1/2}\ .$$

These quantities are plotted on Fig. 5.

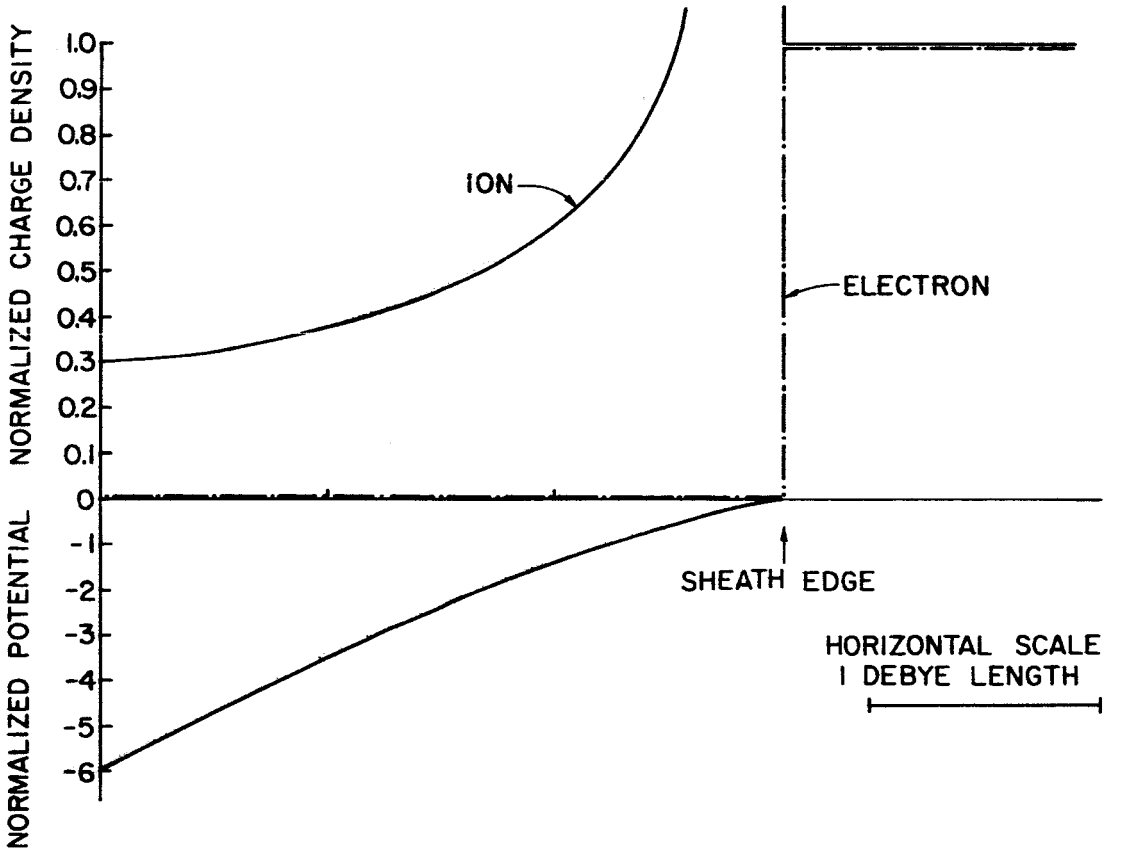

FIG. 5. CHARGE DENSITY AND POTENTIAL PROFILES IN THE SHEATH, MODELS II AND III, PLANAR GEOMETRY.

c. Cylindrical and Spherical Geometries

Similarly the radius of the sheath is found by equating the ion flow to the electron flow. For example, in cylindrical geometry, the ion current is written,

$$I_p = \frac{8}{9} \pi \epsilon_o \left(\frac{2e}{M}\right)^{1/2} \frac{(-V_o)^{3/2}}{\beta^2} \frac{\ell}{r_o} ,$$

where β has been tabulated as a function of r_1/r_o by Langmuir and Blodgett.[24]

The random electron flux is again given by Eq. (6). Equating the two currents, one computes β and finds r_1/r_o from the table mentioned above. The sheath capacitance is then found from

$$C_s = \frac{2\pi\epsilon_o \ell}{\ln \frac{r_1}{r_o}} . \qquad (26)$$

The spherical geometry is treated in a similar way, the computations involving another constant β which has been also tabulated by Langmuir and Blodgett.[25]

4. Theoretical Determination of the Sheath Capacitance, Model III

This model is borrowed from Butler and Kino.[20] The initial assumptions and the charge distribution in the sheath are the same as in Model II and again we assume that the ion current to the probe is limited by the space charge in the sheath.

From Eq. (22) the sheath thickness is written

$$d = \frac{2}{3}\left(\frac{\epsilon_o A}{I_p}\right)^{1/2}\left(\frac{2e}{M}\right)^{1/4}(-V_o)^{3/4} ,$$

when the potential of the probe varies, the sheath edge moves with a velocity

$$\frac{\partial d}{\partial t} = \frac{1}{2}\left(\frac{\epsilon_o A}{I_p}\right)^{1/2}\left(-\frac{2e}{MV_o}\right)^{1/4}\frac{\partial V_o}{\partial t} ,$$

the ion current, I_p, is not a function of time since it is assumed that the ions cannot follow the alternating field.

The periodic variation of the sheath thickness is equivalent to an electron current given by

$$\text{Ane}\ \frac{\partial d}{\partial t} = C_s \frac{\partial V_o}{\partial t} ,$$

replacing for $\partial d/\partial t$ we find

$$C_s = A \frac{ne}{2} \left(\frac{\epsilon_o A}{I_p} \right)^{1/2} \left(- \frac{2e}{MV_o} \right)^{1/4} .$$

Computing I_p from Eqs. (6) and (7), we obtain at floating potential

$$C_s = \epsilon_o \frac{A}{\lambda_D} \left(\frac{4M}{\pi m} \frac{-V_f}{V_e} \right)^{-1/4} \exp \left(- \frac{V_f}{2V_e} \right) \qquad (27)$$

Taking into account Eq. (8), Eq. (27) is written

$$C_s = \epsilon_o \frac{A}{\lambda_D} \left(-8 \frac{V_f}{V_e} \right)^{-1/4} . \qquad (28)$$

Comparing Eqs. (12) and (28) we obtain

$$\gamma = (-8y_f)^{-1/4} = 0.594 \ (-y_f)^{-1/4} . \qquad (29)$$

5. Theoretical Determination of the Sheath Capacitance, Model IV

This model has already been given by Crawford and Grard;[26] the initial assumptions are the same as in Bohm's theoretical determination of the floating potential. From Eq. (5) we know that the derivative of the potential in the sheath can be written

$$\frac{\partial V}{\partial r} = \left(\frac{2ne}{\epsilon_o} \right)^{1/2} \left[2[V_i(V_i - V)]^{1/2} - 2V_i - V_e \left(1 - \exp \frac{V}{V_e} \right) \right]^{1/2} .$$

At the probe surface, we have

$$\left(\frac{\partial V}{\partial r} \right)_o = \frac{(2V_e)^{1/2}}{\lambda_D} \left[[V_i(V_i - V_o)]^{1/2} - \left(V_i + \frac{V_e}{2} \right) \right]^{1/2} ,$$

where $\exp (V_o/V_e)$ has been neglected with respect to unity.

Assuming that the ion density can follow the variation of the ac field and making use of Eq. (11), we obtain for the sheath capacitance

$$C_s = \epsilon_o \frac{A}{\lambda_D} \frac{1}{2} \left[\frac{V_i}{V_e} \left(\frac{V_i - V_o}{V_i} \right)^{3/2} - \left(\frac{V_i}{V_e} + \frac{1}{2} \right) \frac{V_i - V_o}{V_i} \right]^{-1/2} . \qquad (30)$$

If we assume that the ions enter the sheath with an energy $eV_e/2$ and if we make use of Eq. (12), we reach the following result for the normalized capacitance

$$\gamma = \frac{1}{2} \left[\frac{1}{2}(1 - 2y_o)^{3/2} - (1 - 2y_o) \right]^{-1/2} . \qquad (31)$$

Numerical integration of Eq. (4) on a computer yields the normalized quantities V/V_e, n_e/n and n_i/n. The profiles of these quantities in the sheath are shown on Fig. 6.

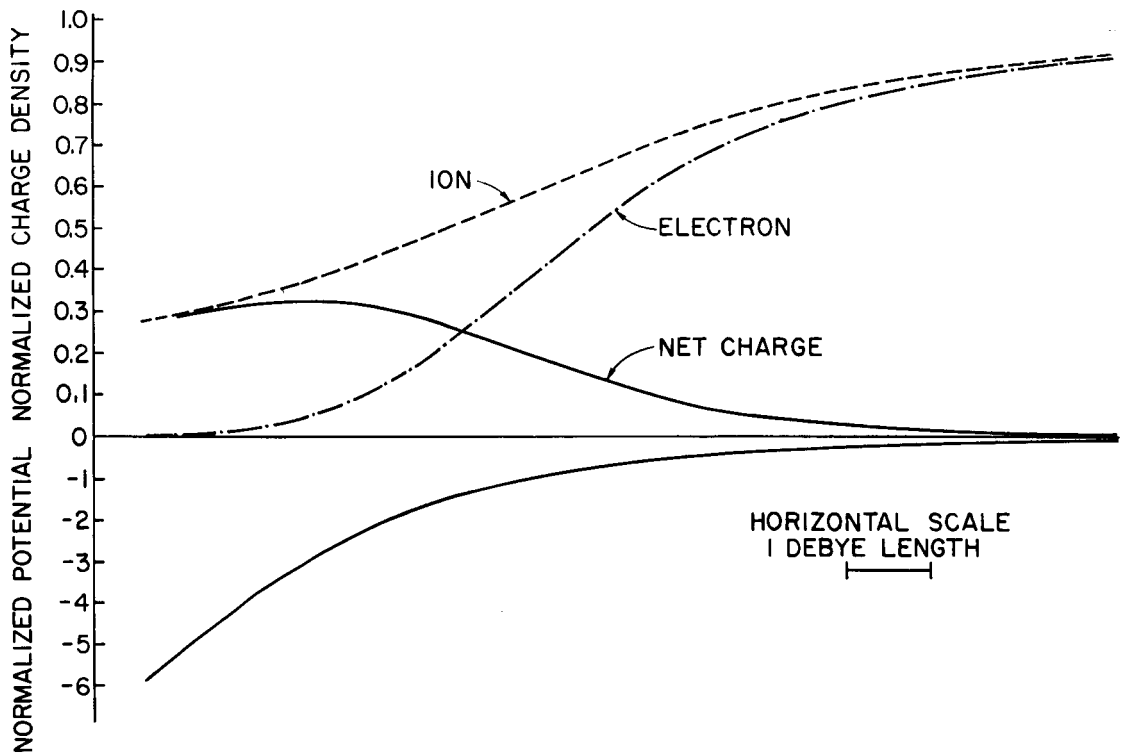

FIG. 6. CHARGE DENSITY AND POTENTIAL PROFILES IN THE SHEATH, MODEL IV, PLANAR GEOMETRY.

E. DISCUSSION

1. Comparison Between the Different Models

In the first three models it is assumed that the time variation of potential is too rapid for the ions to follow. In Model I, the acceleration of the ions in the sheath by the dc field is neglected but the electron density is fairly well described by Boltzmann's law. In Models II and III the acceleration of ions is taken into account although there is some inconsistency at the sheath edge because the Child-Langmuir law assumes that the ions are emitted without initial velocity while Bohm's theory assumes that they enter the sheath with an energy equal to $eV_e/2$. The profile of the electron density is discontinuous at the sheath edge.

In order to see under what conditions these assumptions are justified, one can examine Fig. 6 which displays the most realistic charge density profiles.

It can be seen that Model I must be used for slightly negative potential when it is not permissible to adopt a discontinuous profile for the electron density and when the ion acceleration is small. Contrarily, Models II and III are preferred when the probe is very negative. Then the rarefaction of ions due to their acceleration is important but the electron content of the sheath is small with respect to the ion content. The error made in the computation of the sheath capacitance by taking a discontinuous electron profile can be estimated by comparing Eqs. (17) and (20). This error effectively decreases when the potential of the probe becomes more and more negative. This relative error is less than 6 percent in the case of a probe at floating potential in a mercury plasma.

In Model IV, it is assumed that both ions and electrons respond without appreciable delay to the alternating potential when the frequency of the ac signal is sufficiently low.

The variations of γ with y_f are plotted for each model on Fig. 7. The range of y_f values is suitable for gases of atomic masses between 1 and 200.

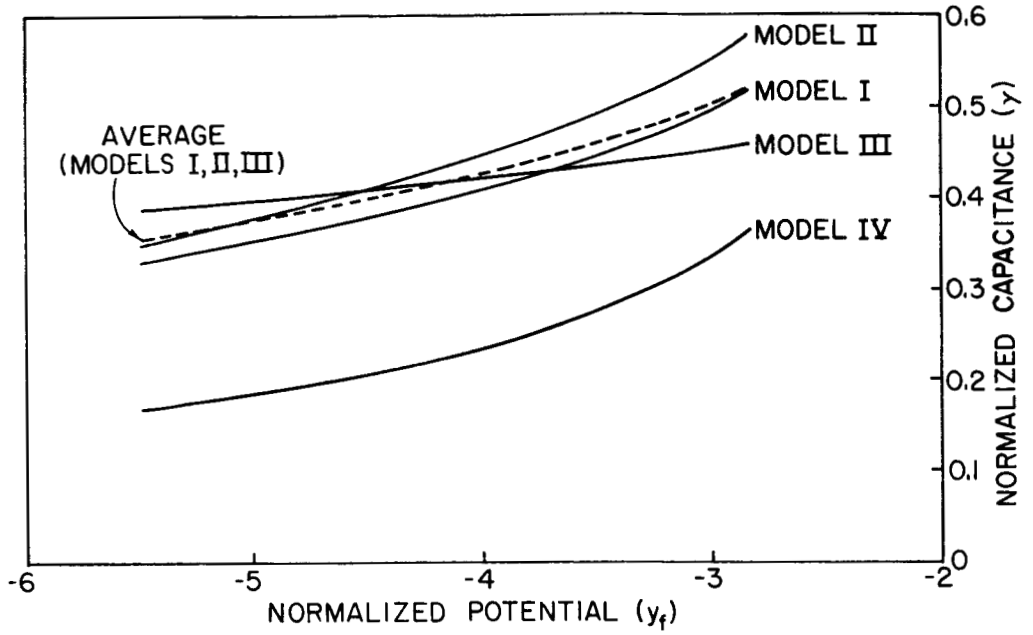

FIG. 7. NORMALIZED SHEATH CAPACITANCE FOR DIFFERENT MODELS, PLANAR GEOMETRY.

It is satisfying that the first three models, valid in the upper frequency range, give very similar results notwithstanding the differences between the initial assumptions. Model IV, which describes the behaviour of the sheath at lower frequencies, gives values of γ approximately half of those found from the previous models. One must note that Eqs. (25) and (29) are only valid for a probe at floating potential while Eqs. (17) and (31) are also valid for a biased probe. We cannot say a priori what frequency delimits the ranges of application of Models I, II and III on one hand, and Model IV, on the other hand. We will approach this problem from an experimental standpoint.

2. Effect of a Magnetic Field

The interaction of a magnetic field with a moving probe was first studied by Beard and Johnson.[27] For instance, if an electromotive force is induced by the earth's magnetic field in a cylindrical probe moving in the ionosphere, the Laplacian of the potential becomes

$$\nabla^2 V = \frac{1}{r}\frac{\partial}{\partial r}\left(r\frac{\partial V}{\partial r}\right) + \frac{\partial^2 V}{\partial z^2} .$$

This equation reduces to a one dimension problem only when $\partial^2 V/\partial z^2$ is negligible. Then the distributed capacitance is independent of z and the total capacitance is found by an integration.

Although a magnetic field does not perturb the velocity distribution function of the components of an infinite plasma, it does affect the collection of these particles by a probe. An approach to this problem was undertaken by Zachary[28] but his results, which are in integro-differential form, are not yet suitable for numerical applications. A more direct attempt was made by Fontheim, Hoegy, Kanal and Nagy.[29] They assumed that the particles are emitted at the sheath edge with a Maxwellian velocity distribution function. Their study is limited to the case of a cylindrical probe in the presence of an axial magnetic field. They found that, if the potential is retarding, the random current to the probe is unaffected by the magnetic field when

$$|y_o| \geq \frac{r_1^2 - r_o^2}{4}\left(\frac{\omega_c}{v_o}\right)^2 ,$$

where, $y_o = eV_o/kT$ is the normalized potential of the probe, r_o and r_1 are respectively the probe and sheath radii, ω_c is the cyclotron angular frequency and v_o is the particle thermal velocity.

III. EXPERIMENTAL STUDY OF THE SHEATH IN THE LABORATORY

This is a description of the laboratory experiments carried out to verify the validity of the theory presented in the preceding chapter.

A. THE ARC DISCHARGE

1. The Tube

The tube is made of a sealed pyrex cylinder one meter long and six centimeters in diameter. This tank has been emptied of air and filled with a saturated mercury vapor. At the ends of the tube are the cathode and the anode: the cathode is coated with an oxide and heated by a tungsten filament; the anode is made of a hollow cylinder. The tube is shown in Fig. 8. The filament is supplied with 35 watts dc power from a battery charger. The anode is connected to a regulated power supply; when a dc potential of about 200 volts exists between the extremities of the tube, a discharge can be established with a Tesla coil. After ignition, the difference of potential between anode and cathode drops to 36 volts; a series 2.5 kΩ resistance limits the current.

2. The Plasma

We determine the characteristics of the plasma in the positive column by the Langmuir technique. Using Eq. (6) and neglecting the ion current, we may write the logarithm of the random current collected by the probe as

$$\ell n\ I = \frac{V_o}{V_e} + \ell n\ I_{se} \ .$$

It follows that $\ell n\ I_e$ varies linearly with the probe potential and that the slope of the curve yields the electron potential, V_e. This relation applies for $V_o \leq 0$. When the probe is at space potential ($V_o = 0$), the current reaches its saturation value, I_{se}, as is shown on Fig. 16. Using Eq. (9), one can obtain the electron density from the saturation current.

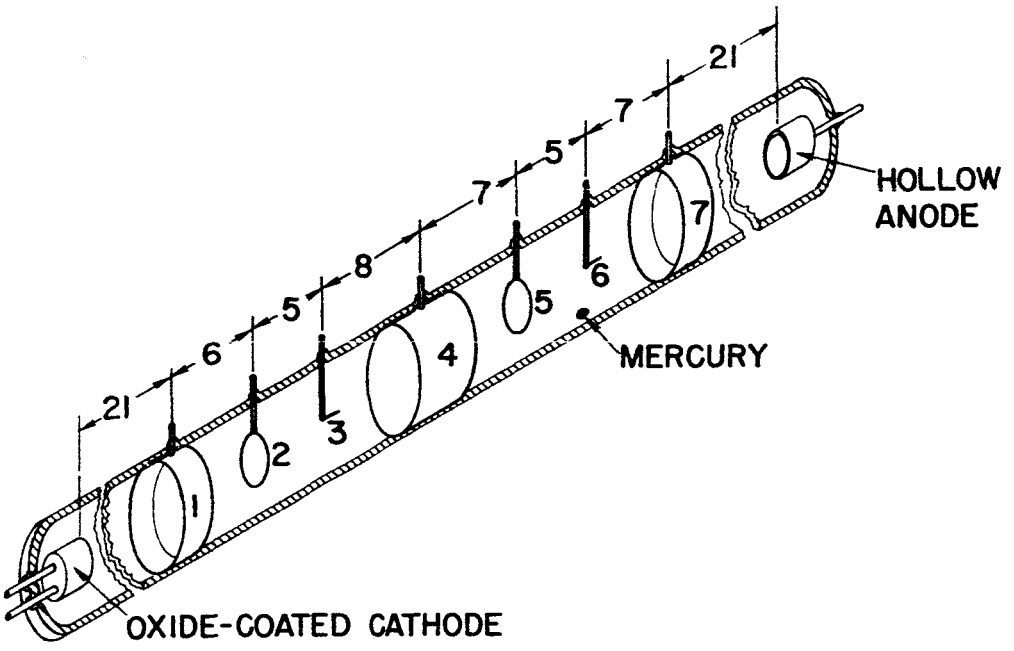

FIG. 8. EXPERIMENTAL MERCURY-VAPOR DISCHARGE TUBE. (Dimensions in cm, tube inside diameter, 6 cm)

Table 1 summarizes the results obtained with four different probes; the dimensions of the probes are given by Table 2. The large collecting area of electrode 2 does not allow one to reach the saturation current without seriously perturbing the discharge.

Other average parameters of the plasma for an arc current of 100 ma are:

electron velocity, $v_e = 8 \times 10^7$ cm/s,

plasma angular frequency, $\omega_p = 1.75 \times 10^9$ s^{-1},

dc resistivity, $\eta = 1.27$ Ω x m,

electron-neutral collision frequency, $\nu = \epsilon_o \eta \omega_p^2 = 3.5 \times 10^7$ s^{-1}

electron-neutral mean free path, $\lambda_c = v_e/\nu = 2.3$ cm.

TABLE 1. PLASMA PARAMETERS DETERMINED WITH DIFFERENT PROBES FOR A 100 MA DISCHARGE CURRENT.

Probe Number	2	5	3	6
V_e: electron potential volts	2.3	2.26	1.59	1.63
T_e: electron temperature, °K	26500	26000	18300	18800
V_f: floating potential, volts		-11.8	-8	-7.2
$y_f = \frac{V_f}{V_e}$		- 5.2	-5	-4.4
I_{se}: saturation current, ma		3.2	2.8	0.23
n: electron density, m^{-3}		1.06×10^{15}	1.37×10^{15}	1.35×10^{15}
λ_D: Debye length, mm		0.338	0.255	0.258

TABLE 2. DETAILS OF THE PROBE ELECTRODES

Probe Geometry	Planar		Cylindrical			
			Loop		Straight	
Probe number	1,7	4	2	5	3	6
Probe width, or wire diameter, d, mm	20	40	2.54	0.254	2.54	0.254
Length, cm	6π	6π	3π	3π	0.75	0.6
Surface area, cm^2	37.7	75.4	7.52	0.752	0.60	0.05
(d/λ_D) at 100 ma tube current	~ 70	~ 140	~ 10	~ 1	~ 10	~ 1

There are some discrepancies between the electron temperature measurements made with the different probes, but good agreement is observed between the results found from electrodes similarly located with respect to the tube axis; electrodes 3 and 6 are on the axis, electrodes 2 and 5 are equidistant from the axis and the wall. However, the existence of a radial gradient of temperature is not in accord with the conclusions of Crawford and Self.[30] For an average room temperature of 30 °C the neutral pressure inside the tube equals 2.8 microns. The mercury vapor pressure doubles with a temperature increase of nine degrees, and room temperature variations as large as 5 °C during one day are common. Then, it is possible that part of the electron temperature discrepancies is due to a variation of the neutral pressure. An alternative explanation is that some electrodes are perturbing the plasma when their potential is positively biased towards the space potential. Having a large collecting area, they draw a current which cannot be neglected.

The values of the normalized floating potential, y_f, compares favorably (within 20 percent) with the theoretical determination of Bohm's.

There is a 22 percent drop in the electron density from the axis of the tube (electrodes 3 and 6) to a point half-way between the axis and the glass wall (electrodes 2 and 5). In a cylindrical tube where the ratio of the diameter over the Debye length on the axis equals roughly 250, Parker[23] suggested that a fall-off of 18 percent should occur.

The electron density at the sheath edge against the wall is not known but can be computed from the density on the axis. After Bohm, we assume that the ions entering the sheath have an energy $(eV_e/2)$ and that, consequently, there is a potential drop of $(V_e/2)$ between the axis and the wall sheath. Applying Boltzmann's law, we find that the electron density at the sheath edge is $1.36 \times 10^{15} \exp(-1/2) = 0.825 \times 10^{15}$ (m^{-3}); this estimate is about 40 percent higher than Parker's prediction. The electron density varies linearly with the discharge current but the electron temperature does not vary significantly with the tube current.

3. Impedance of the Plasma Column

The impedance of a mercury plasma column, computed by Crawford,[31] is given by

$$Z_t = \frac{j\omega R_o}{\nu} \frac{\nu + j\omega}{b + j\omega} ,$$

where R_o is the dc resistance of the tube and ω is the angular frequency. The value of the constant b can be shown to be

$$b = \frac{2}{a} \left(\frac{eV_e}{M}\right)^{1/2} ,$$

where a is the radius of the tube.

In the conditions of our experiment we have approximately: $b = 1.5 \times 10^5 \ s^{-1}$, $\nu = 3.4 \times 10^7 \ s^{-1}$ and $\omega < 4\pi \times 10^6 \ s^{-1}$.

The admittance of the column can be written

$$\frac{1}{Z_t} = \frac{\nu}{R_o} \frac{\nu - b}{\nu^2 + \omega^2} - j \frac{\nu}{\omega R_o} \frac{b\nu + \omega^2}{\nu^2 + \omega^2} ,$$

which can be simplified to

$$\frac{1}{Z_t} = \frac{1}{R_o} - j \frac{1}{R_o} \left(\frac{b}{\omega} + \frac{\omega}{\nu}\right) ,$$

by taking into consideration the orders of magnitude of b, ν and ω.

Consequently, over our range of approximations, the parallel ac resistance of the tube equals its dc resistance. We find experimentally that the parallel ac resistance of the column is fluctuating between 370 Ω and 490 Ω when the frequency varies from 0.1 Mc/s to 1.6 Mc/s, while its dc resistance equals roughly 360 Ω. Experimentation shows also that the parallel ac reactance of the column is at least four times larger than the resistance.

B. EXPERIMENTAL EQUIPMENT

1. The Probes

Electrodes 1, 4 and 7 are made of metallic cylinders lining the inside wall of the tube; we consider these electrodes as being planar because their width and radius of curvature are much larger than the Debye length. Electrode 4 is coated with an insulator (alumina) to avoid perturbing the longitudinal gradient of the potential. Electrodes 3 and 6 are made of cylindrical tungsten wires parallel to the axis of the tube.

Electrodes 2 and 5 have the shape of a torus centered on the axis of the tube; these probes will be treated as cylinders also because the diameter of the loop is much larger than both the Debye length and the diameter of the wire.

The supports of electrodes 2, 3, 5 and 6 are surrounded by a shielding cylinder which is itself coated with glass, as shown on Fig. 9. From a practical point of view it has been very difficult to limit the glass coating to the support alone and roughly one third of electrodes 3 and 6 was also covered with glass. However, this perturbing effect is negligible for probes 3 and 6 and therefore we can expect much more accurate results from these electrodes.

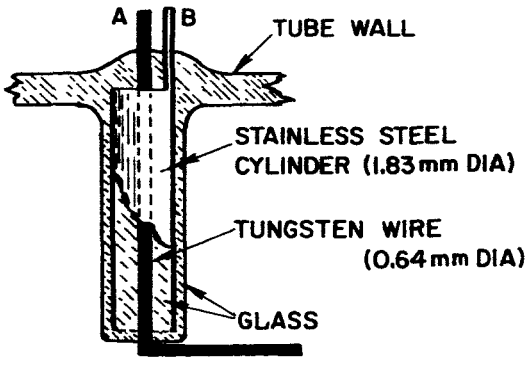

FIG. 9. DETAILS OF THE SCREENED SUPPORT OF A PROBE.

The shielding effect of the cylinder which surrounds the probe support is explained on Fig. 10 where

C_o = the capacitance between the central conductor and the cylinder,

Z_s = the sheath impedance of the probe,

Z'_s = the sheath impedance of the support, and

Z_p = the impedance of the plasma column.

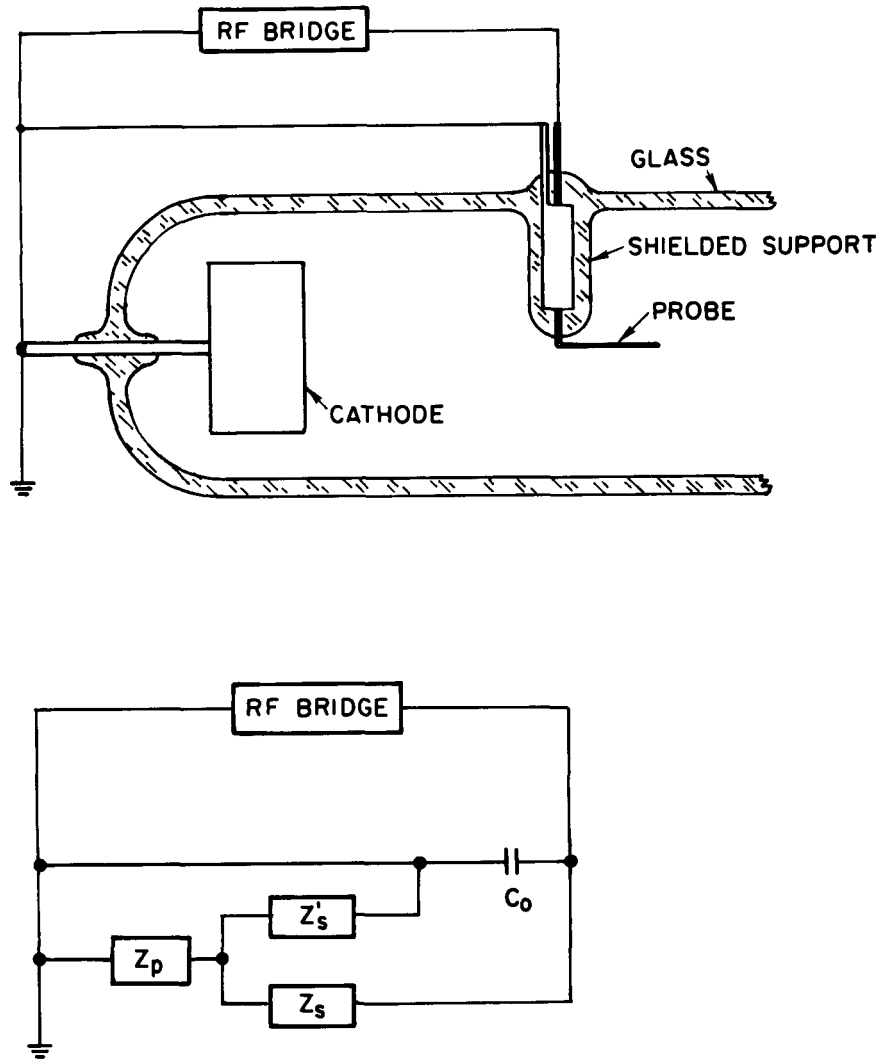

FIG. 10. A REPRESENTATION OF THE SYSTEM UTILIZED TO SHIELD THE SUPPORT AND CORRESPONDING CIRCUIT DIAGRAM.

The sheath impedance of the support is effectively short-circuited by the much lower impedance of the plasma column and the capacitance C_o can be easily measured or taken into account in the initial balance of the bridge.

2. The Measurement Circuit

A simplified representation of the circuit is shown on Fig. 11. The anode is connected to the ground by a large capacitor which offers a low impedance to the alternating signal. The total ac impedance between probe and ground is

$$Z = Z_s + \frac{Z_a Z_k}{Z_a + Z_k} ,$$

where Z_a and Z_k are, respectively, the probe-anode and probe-cathode plasma column impedances.

The second term is maximum when the probe is located at the same distance from the anode as from the cathode, then $Z_a = Z_k = Z_t/2$ and $Z = Z_s + Z_t/4$.

We know that $Z_t \simeq 400\ \Omega$; we will see that $Z_t/4$ is always negligible with respect to Z_s.

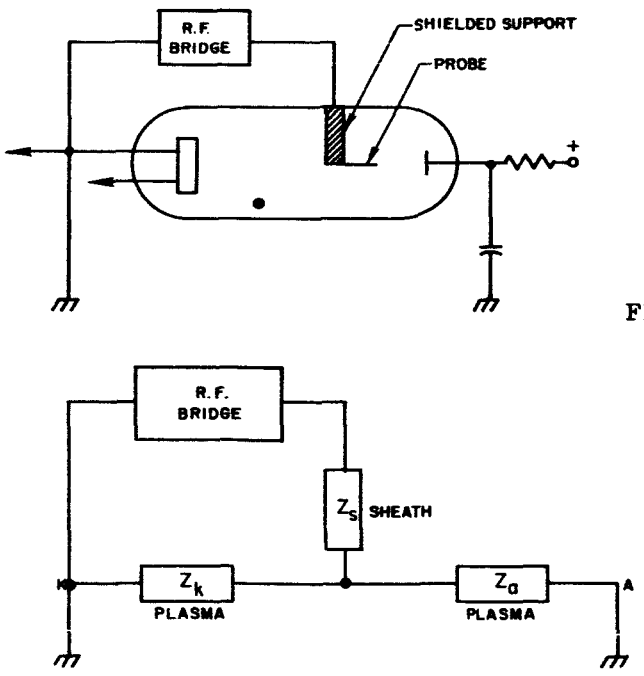

FIG. 11. A SCHEMATIC REPRESENTATION OF THE MEASUREMENT SYSTEM AND CORRESPONDING CIRCUIT DIAGRAM.

The complete measurement circuit is shown on Fig. 12. The potential of the probe can be swept by an auxiliary circuit made of a variable regulated power supply in series with a high resistance, 0.25 MΩ, connected between the probe and the cathode.

The admittance between the probe and the ground is measured with a radio frequency bridge. The signal of a variable frequency generator is injected in the bridge. It is essential that the amplitude of the alternating voltage applied to the probe be small with respect to the electron temperature; otherwise, a detection effect biases the probe to a more negative potential and changes the magnitude of the sheath admittance. This effect has been studied by Butler and Kino.[20]

The bridge equilibrium is detected with a spectrum analyzer. It is very convenient to use a Panoramic spectrum analyzer as a null detector because it allows us to distinguish the ac signal given by the generator from the noise emitted by the plasma tube. It is not possible to eliminate this noise in the bridge balance because it occurs in one of the bridge arms.

The measurement of the admittance is performed in two steps. First, when the tube is turned off, one measures the admittance of the system which sweeps the probe voltage in parallel with the capacity C_o which exists between the probe support and its shield. Secondly, when the tube is ignited, one measures the perturbing admittance mentioned

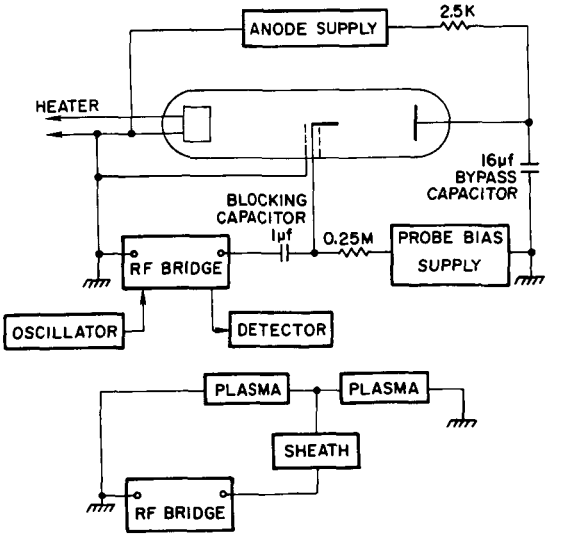

FIG. 12. CIRCUIT USED FOR THE MEASUREMENT OF THE SHEATH ADMITTANCE.

above in parallel with the admittance of the probe itself. The difference between these two measurements yields the probe admittance.

C. SHEATH ADMITTANCE MEASUREMENTS

1. The Sheath Conductance

It can be seen from Fig. 13 that the ion contribution to the incremental sheath conductance is negligible when the probe potential is equal or superior to the floating potential. In fact the variation of the ion current with potential is less than 5 percent of the total current variation around the floating potential. The approximation made in order to obtain Eq. (10) is consequently justified. We must now verify that the principal features of this equation are confirmed by experimentation.

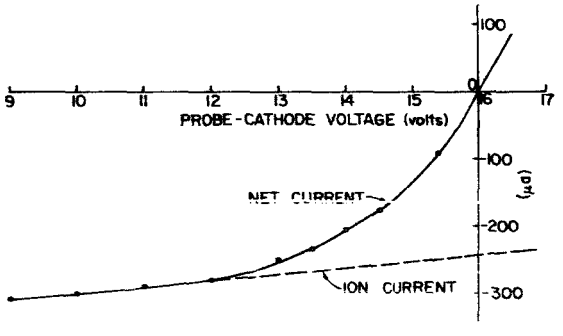

FIG. 13. DC PROBE CHARACTERISTICS BELOW FLOATING POTENTIAL. (Electrode 7, tube current 100 ma)

The sheath conductance was measured over a range of frequency including the ion plasma frequency, f_i = 450 kc/s. Figure 14 shows that the conductance remains constant and equal to the value found by graphical differentiation of the dc Langmuir probe characteristic.

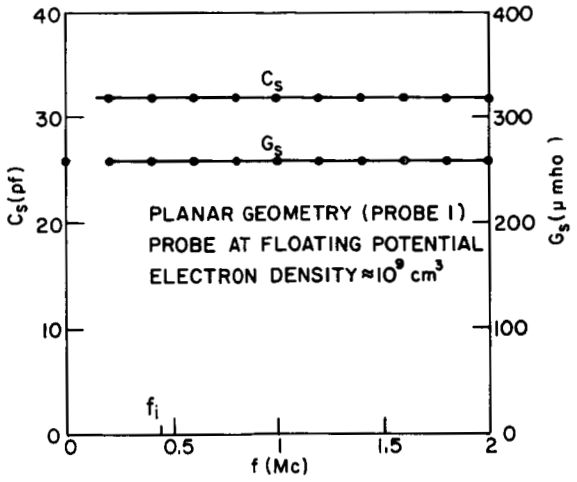

FIG. 14. VARIATION OF SHEATH CONDUCTANCE AND CAPACITANCE WITH FREQUENCY.

The sheath conductance varies linearly with the electron density, which is proportional to the tube current. Supporting results are shown on Fig. 15. Furthermore, one checks that the conductance is geometry independent, since linear variations are observed in planar and cylindrical geometry.

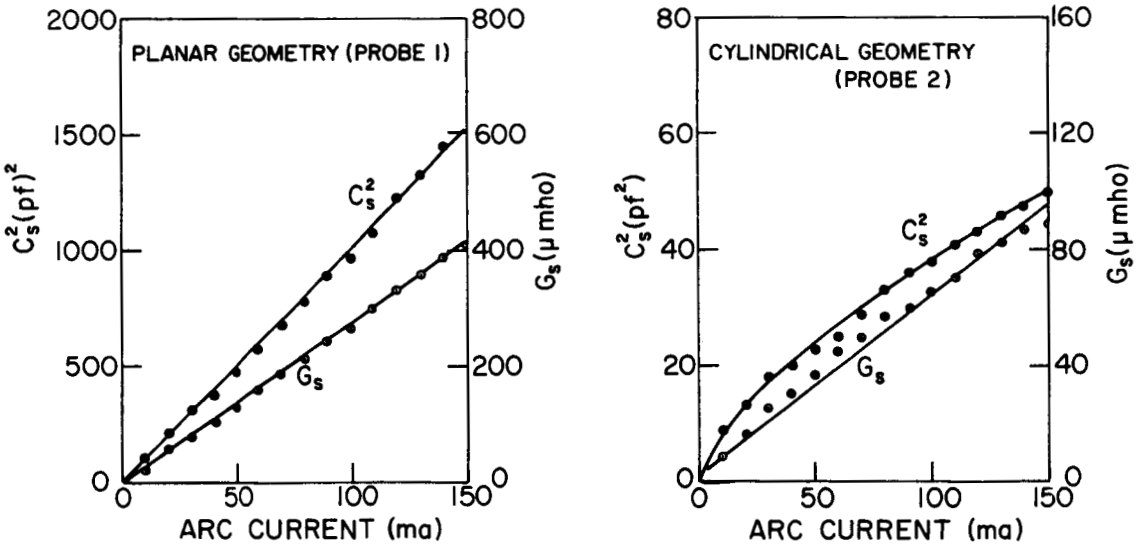

FIG. 15. VARIATION OF THE PROBE CONDUCTANCE AND CAPACITANCE WITH DISCHARGE CURRENT. (Working frequency 500 kc. Probes at floating potential.)

Equation (10) shows also that the conductance is proportional to the probe current. Experiments were carried out to verify this point by biasing the potential of the probe. Results are shown on Fig. 16 and compared to those obtained by using the conventional Langmuir technique. The slope of the curve yields V_e = 2.15 volts which agrees within less than 3 percent with the electron temperature previously determined from the dc characteristic. It must be noted that the electron temperature can be determined from a single measurement of the ac conductance while the Langmuir method requires sweeping a part of the dc characteristic. Equation (10) breaks down at floating potential and the determination of the "breakpoint" gives I_{se} = 3 ma which agrees within 6 percent with the saturation current obtained with the same probe by the Langmuir technique. In order to measure the saturation current with accuracy, it is necessary that the impedance of the plasma column remain negligible with respect to the sheath impedance at floating potential.

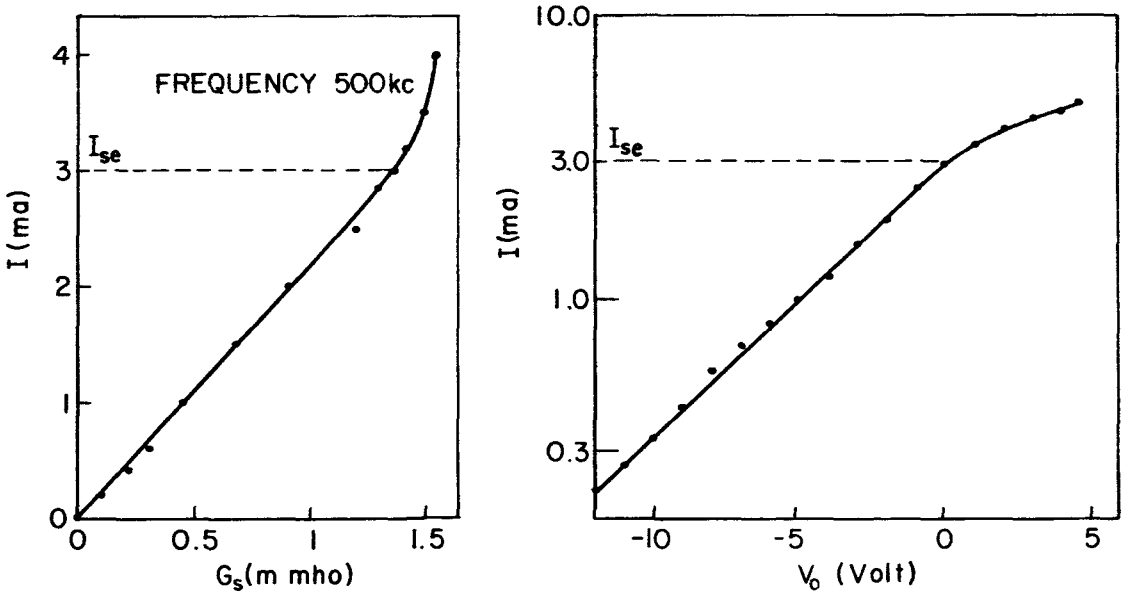

FIG. 16. COMPARISON OF CONDUCTANCE AND CONVENTIONAL LANGMUIR PROBE CHARACTERISTICS. (Cylindrical geometry, probe 5, electron density $\simeq 10^9$ cm^{-3})

From a practical standpoint there are some advantages in using the conductance measurements to locate the space potential. The sheath conductance is reasonably stable in time whereas the dc potential of the probe suffers small erratic fluctuations due to variations of the plasma column resistance. Furthermore, the "breakpoint" is somewhat sharper and can be determined with better accuracy on a linear conductance plot than on a semilogarithmic dc probe characteristic.

Finally, we can compute from Eq. (10) the normalized floating potential of the probes, V_f/V_e, assuming for the electron potential an average value $V_e = 2$ volts. The results are shown on Table III and agree within 20 percent with the results of Table I and Bohms' theoretical determination.

2. The Sheath Capacitance

Figure 14 shows that the capacitance is frequency independent over the same range of frequency as the conductance. This implies that rf ion motions are negligible and suggests that Eqs. (18), (24), and (28), which we know a priori to be valid above the ion plasma frequency, apply also below this frequency. The range of applicability of Eq. (30) cannot be reached with our experimental apparatus. In effect, it is not possible to carry out the measurements at frequencies lower than 100 kc/s because the sheath susceptance becomes negligible with respect to the conductance.

All capacitance models indicate that the sheath capacitance in planar geometry must be inversely proportional to the Debye length. This condition may be expressed as direct proportionality of C_s^2 to the discharge current. Figure 15 shows the effect of current variation. For the planar probe, which is large compared to a Debye length, we see that the proportionality is satisfied. For the cylindrical probe whose diameter does not greatly exceed the sheath thickness, the required proportionality breaks down.

Finally, a direct check of the capacitance is required. Some typical measurements at floating potential are shown on Table III. One notes that the admittance measurements made with electrodes 1 and 7 are different. These electrodes are physically identical but they are

TABLE 3. COMPARISON BETWEEN THE THEORETICAL AND EXPERIMENTAL DETERMINATIONS OF THE SHEATH CAPACITANCE FOR A 100 MA DISCHARGE CURRENT

Probe Number		1	7	2	5
Electron density, m^{-3}		0.825×10^{15}	0.825×10^{15}	1.06×10^{15}	1.06×10^{15}
Debye length, λ_D, mm		0.366	0.366	0.323	0.323
$x_o = r_o/\lambda_D$		∞	∞	3.93	0.393
Measured sheath conductance, μmho		260	185	66.6	15
$y_f = V_f/V_e$		-5.39	-5.75	-5.41	-4.60
Computed sheath capacitance pf	Model I	31	30	9.5	2.72
	Model II	32	27	9.35	2.8
	Model III	34	39	--	--
	Model IV	19	18	--	--
Measured sheath capacitance, pf		32	25	6.3	2.35

located at opposite ends of the positive column. It is possible that a lack of uniformity of the plasma parameters is responsible for these differences.

The predicted values of the capacitances are found from Eqs. (18), (23), (27), and (30) in planar geometry (electrodes 1 and 7), and from Eqs. (19) and (26) in cylindrical geometry (electrodes 2 and 5). We used an average value for the electron temperature, $V_e = 2$ volts, and we determined V_f/V_e from the conductance measurements. The predictions

from Models I, II, and III are slightly too large and the average discrepancy for the planar probes equals 4pf. The predictions in cylindrical geometry are, on the average, 50 percent and 18 percent too high, respectively for electrodes 2 and 5. The discrepancies can be explained by the simplifications made in the conventional Langmuir probe data reduction on which the comparison is based. The predictions from Model IV are too small and it seems that we have to disregard this model in the frequency range of our measurements.

D. DISCUSSION

The conductance measurements of a biased probe, which are displayed on Fig. 16, give electron density and temperature. This method has some advantage with respect to the classic Langmuir technique but sweeping the probe potential is still required. Measurements of the electron temperature, which is obtained from a single point of the characteristic, can be made continuously, however.

The admittance measurements at floating potential are particularly simple and are also suitable for continuous measurement but are only appropriate where the electron velocity distribution function is approximately Maxwellian up to energies corresponding to floating potential. The conductance measurements are very sensitive to this requirement but yield a fairly good determination of the space potential.

Though we were able to predict the magnitude of the capacitance from the plasma parameters with reasonably small discrepancies, it is more difficult, inversely, to obtain the electron density from the capacitance with a good accuracy. In effect, n which is proportional to C_s^2, is very sensitive to the simplifications made in the theoretical computation of the sheath capacitance.

However, the proportionalities of G_s and C_s^2 to n have been checked by experiment and one can make use of these properties to record continuously the relative variations of the electron density. We assume that the results can be calibrated by an independent method and that the electron temperature is simultaneously recorded with a biased probe.

If we assume that the smallest capacitance which can be measured with reasonable accuracy, say 10 percent, is 1 pf, we see from Fig. 15 that the smallest electron density which can be detected with an electrode such as probe 1 is 10^6 cm^{-3}.

Continuous measurements are particularly interesting in time-varying plasmas and in space applications where the probe is traveling in a non-uniform medium. However, the sheath must always have time to adjust itself to the ambient conditions before the ac incremental theory applies. The minimum period of adjustment for small variations of the plasma parameters can be estimated from the time required by an ion to travel a distance of 3 Debye lengths which is approximately the thickness of the sheath

$$3 \frac{\lambda_D}{v_i} = \frac{3}{\omega_{pi}} \frac{V_e}{2V_i} ,$$

where ω_{pi} is the ion plasma frequency. This time has the order of magnitude of the ion plasma relaxation period, if we assume $V_e = 2V_i$ at the sheath edge.

Continuous evaluation of the sheath admittance cannot be evaluated with a bridge method in which a finite time is required for the sampling. Instead, the probe voltage and current are recorded on magnetic or photographic tape and the admittance is determined by subsequent data processing.

Another interesting feature of the admittance probe is that, in principle, measurements can be made without any probe inside the tube. In effect one can make an electrode by carefully wrapping a piece of aluminum foil around the tube. The impedance which is measured between this electrode and the ground is due to the dielectric effect of the glass wall in series with the impedance of the sheath which lines the inside of the tube. Knowing the dielectric constant and the thickness of the glass allows one to obtain the sheath impedance at floating potential.

IV. IMPEDANCE PROBE MEASUREMENTS IN THE IONOSPHERE

A. DESCRIPTION OF THE EXPERIMENT

1. The Probe

A rocket was fired from Wallops Island during the night of July 9, 1963. The flight lasted 455 seconds and the peak altitude was 205 km. The payload, designed at Stanford Research Institute, by Orsak and his co-workers[18] included a very low frequency impedance probe.

The probe was made of two flat strips attached to the outside of the nosecone. This nosecone was made of fiber glass of thickness 1.6 mm. Figure 17 illustrates the configuration of this symmetric dipole, the length and width of the electrodes are respectively $L = 107$ cm and $h = 2.54$ cm. In first approximation we will assume that the rocket is a perfect cylinder of diameter $D = 33$ cm and that the strips are parallel.

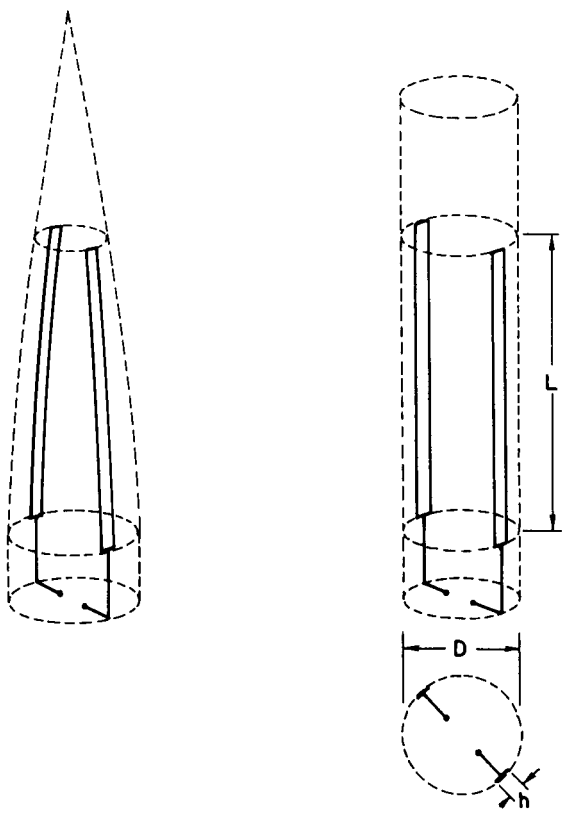

FIG. 17. MODEL OF THE DIPOLE AND ITS APPROXIMATION.

The admittance of the dipole was found from the ratio of the constant alternating current injected into the probe over the voltage measured between the terminals. This voltage equaled at the most 10 mV. It always remained much smaller than the electron potential, and had no perturbing effect on the floating potential of the strips.

The rocket was rotating about its axis with an angular velocity of 2.9 revolutions per second. The angle made by the rocket axis and the earth's magnetic field equaled roughly 30° during the flight.

2. The Data

The admittance measurements were made at two frequencies, 1.54 kc/s and 120 kc/s, and transmitted to the ground at the rate of 14 samples per second for each frequency.

The plots of the measured conductance and capacitance are taken from Orsak's report and are shown on Figs. 18 - 21. They show a very strong dependence on the electron density, and offer a very good spatial resolution which allows us to pinpoint the sporadic E layer and even to distinguish elementary layers less than 1 km thick within the E_s layer itself. The conductance of the dipole was negligible with respect to the susceptance at 120 kc/s and only the susceptance was measured.

One notes that the capacitance and conductance measured at 1.54 kc/s below 90 km during the ascent are surprisingly large. This was tentatively attributed by the experimenters to contamination of the nosecone during its travel across the dense layer of the atmosphere. If this effect were due to the ionization of the medium, which is improbable at this altitude during the night, it would increase with altitude; it would also appear during the descent and would affect in a similar way the measurements made at 120 kc/s.

If one disregards the measurements made at the lower frequency during the ascending part of the trajectory, one notes that the conductance is negligible below 100 km; this proves that the ionization of the ambient gas could not be detected by the probe. The corresponding capacitance has an average value of 15 pf and is practically equal to the free space capacitance for the dipole.

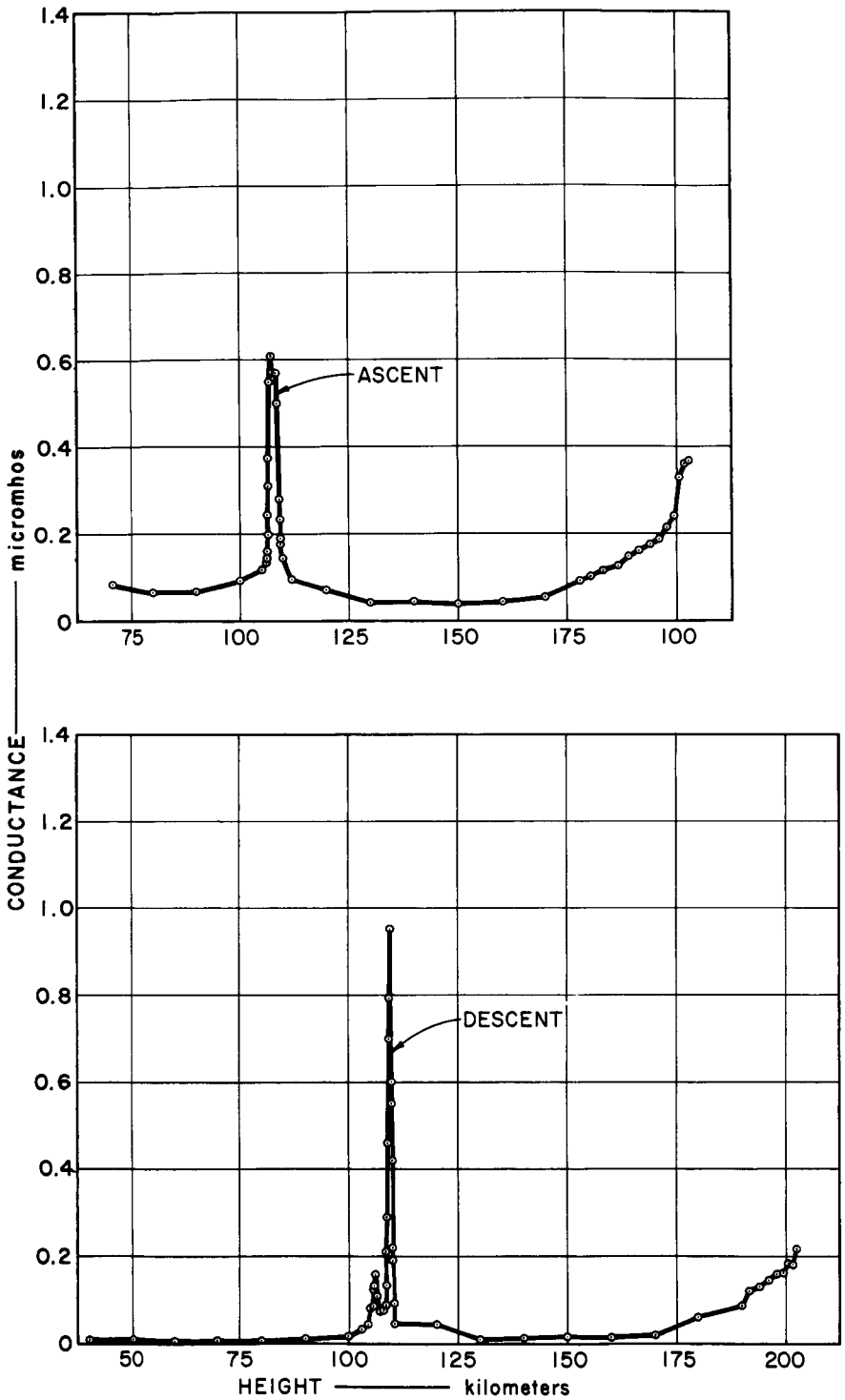

FIG. 18. IMPEDANCE PROBE CONDUCTANCE DATA, 1.54 KC. (Courtesy of L. E. Orsak, L. H. Rorden, G. B. Carpenter and B. P. Ficklin, Stanford Research Institute, Final Rept., Contract NASr-49(01), Jan 1965.)

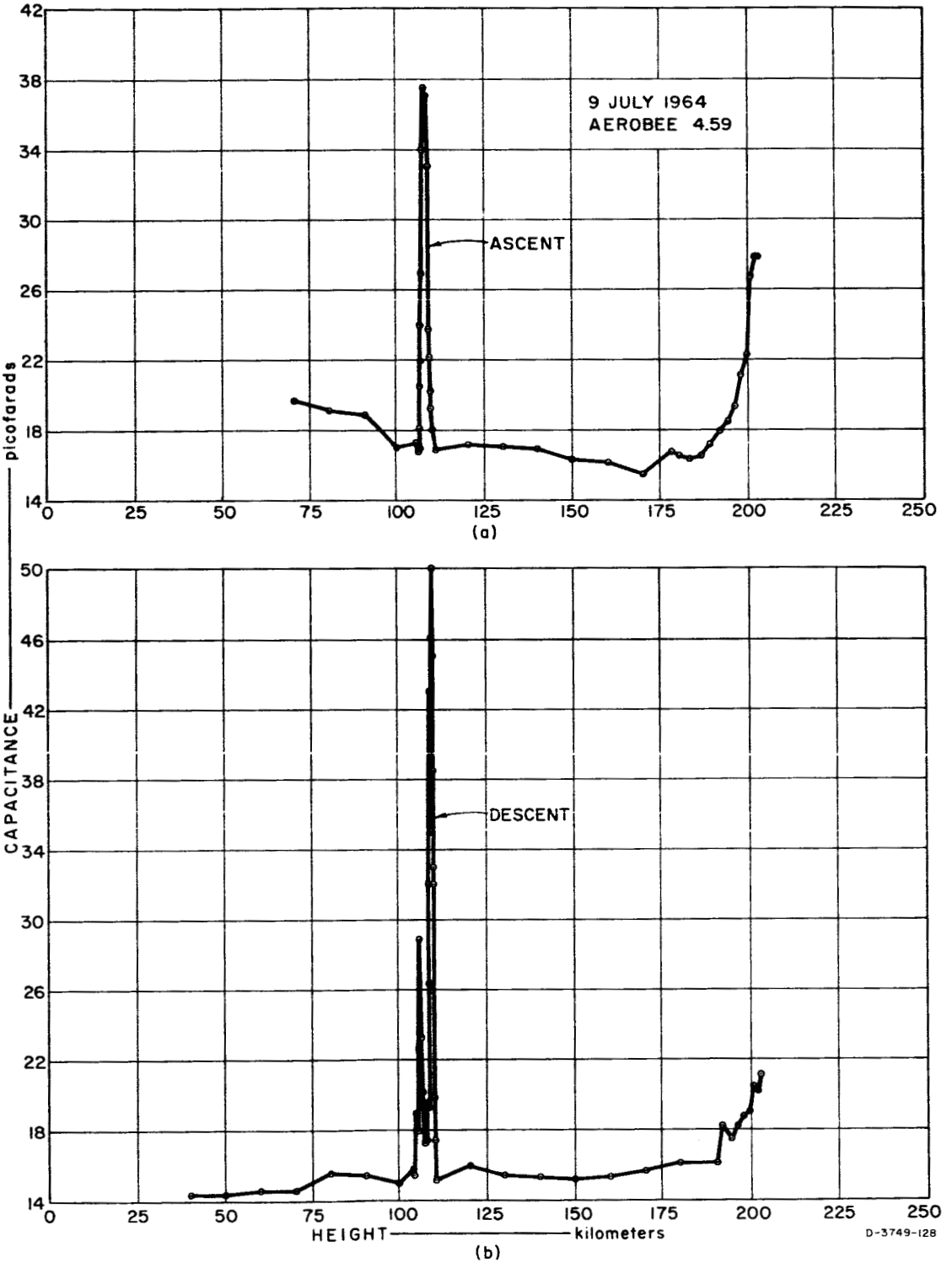

FIG. 19. IMPEDANCE PROBE CAPACITANCE DATA, 1.54 KC. (Courtesy of L. E. Orsak, L. H. Rorden, G. B. Carpenter and B. P. Ficklin, Stanford Research Institute, Final Rept., Contract NASr-49(01), Jan 1965.)

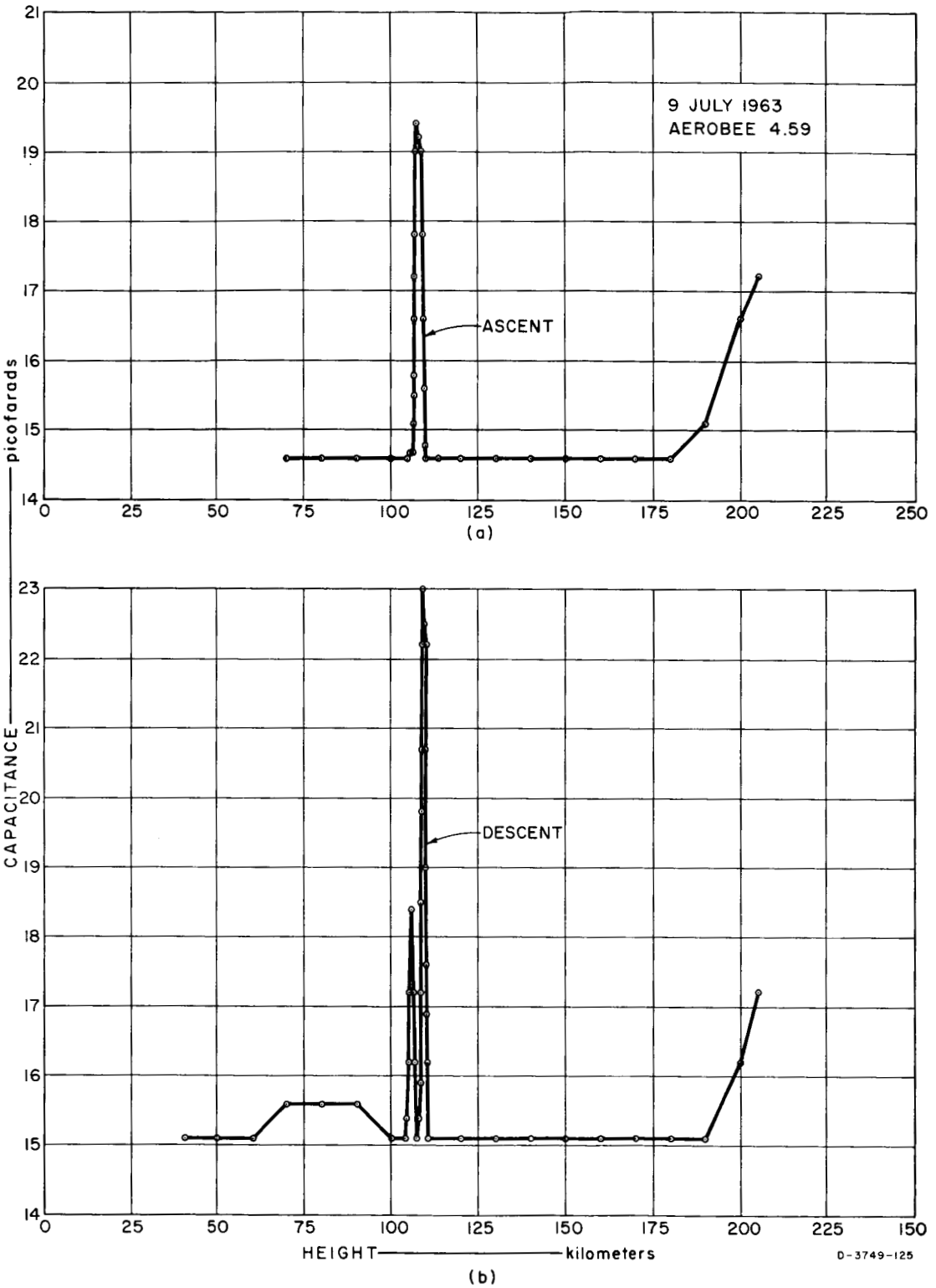

FIG. 20. IMPEDANCE PROBE CAPACITANCE DATA, 120 KC. (Courtesy of L. E. Orsak, L. H. Rorden, G. B. Carpenter and B. P. Ficklin, Stanford Research Institute, Final Rept., Contract NASr-49(01), Jan 1965.)

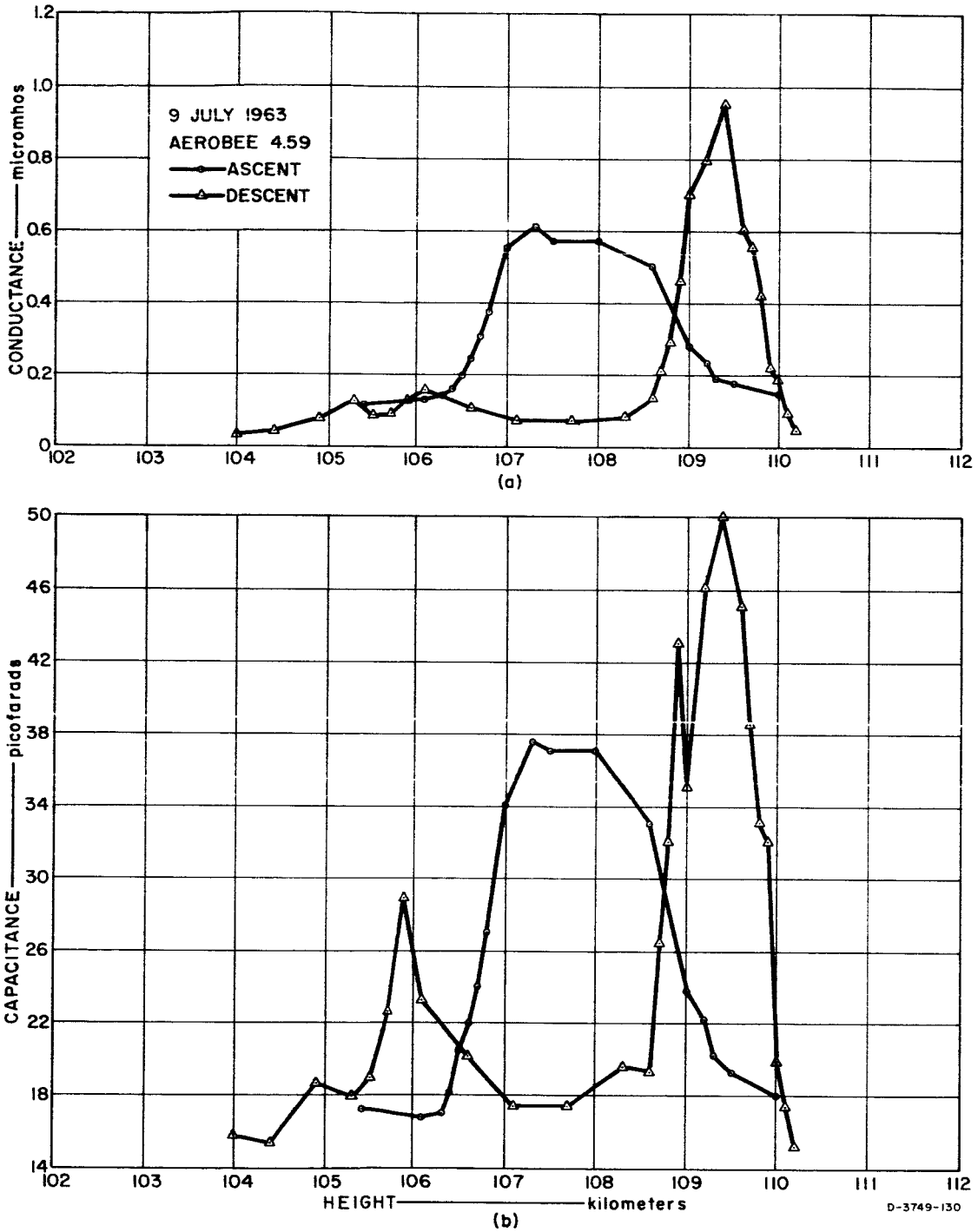

FIG. 21. IMPEDANCE PROBE CONDUCTANCE AND CAPACITANCE IN THE SPORADIC E LAYER. (Courtesy of L. E. Orsak, L. H. Rorden, G. B. Carpenter and B. P. Ficklin, Stanford Research Institute, Final Rept., Contract NASr-49(01), Jan 1965.)

The electron density was measured during the flight with a cw propagation method, and it appears that the probe was not sensitive to electron densities lower than 10^9 m^{-3}.

3. The Components of the Impedance

The impedance of the dipole, as shown on Fig. 22, can schematically be divided into 3 components. The first one, Z_s, is the impedance of the sheath which separates the outer surface of the strips from the plasma. The second component, Z_p, represents the contribution of the plasma which surrounds the probe. The third impedance is due to the internal capacitance, C_i, coupling the two strips through the body of the rocket.

An accurate evaluation of C_i is not feasible because the rocket body is not homogeneous. However, we will determine bounds to its magnitude as follows.

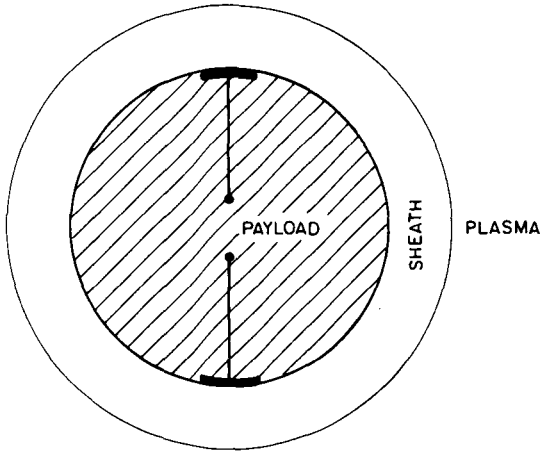

FIG. 22. A SCHEMATIC REPRESENTATION OF THE DIPOLE SECTION AND ITS APPROXIMATION.

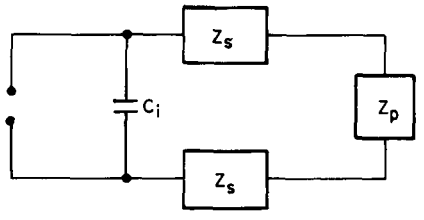

In order to set an upper limit for C_i, we may assume that every electric field line ends on the inner part of the strips and that the coupling takes place entirely through the rocket body. Then C_i equals the total capacitance of the dipole measured in free space.

We can determine a lower limit for the internal coupling by assuming that the charge distribution on one electrode is not influenced by the presence of the other electrode. Then the charge borne by the inner surface of one strips equals very closely the charge borne by its outer surface and C_i equals approximately half of the total free space capacitance.

Consequently, we will write $C_i = 11 \pm 4$ pf.

B. EVALUATION OF THE PLASMA IMPEDANCE

1. Approach to the Problem

We must estimate the contribution of the plasma to the total dipole impedance measured in the ionosphere. We assume that the medium is homogeneous, i.e., we neglect the rarefaction of ions and electrons in the sheath and in the wake.

One approach to this problem is to write for the probe capacity

$$C_p = \frac{\int_S \sigma dS}{V} = \frac{\int_S \overleftrightarrow{\epsilon}_p \vec{E} \cdot \vec{dS}}{V} \qquad (32)$$

where S is the probe surface area, σ is the surface charge density, $\vec{E}$ is the electric field displacement, and $\overleftrightarrow{\epsilon}_p$ is the complex permittivity tensor which includes the effects of magnetic field and collisions.

The ratio of the capacitance with plasma present, C_p, to that with free space as dielectric, C_o, is

$$\frac{C_p}{C_o} = \frac{\int_S \overleftrightarrow{\epsilon}_p \vec{E} \cdot \vec{dS}}{\epsilon_o \int_S \vec{E} \cdot \vec{dS}} \qquad (33)$$

This approach was used by Herman;[32] unfortunately, he assumed that the electric field was the same in both numerator and denominator. This simplification can be employed only if the electric field is everywhere parallel or perpendicular to the magnetic field, then Eq. (33) simplifies to

$$\frac{C_p}{C_o} = \frac{\epsilon_p}{\epsilon_o} ,$$

where ϵ_p must be replaced respectively by the relative permittivity parallel, ϵ_L, or perpendicular, ϵ_T, to the magnetic field.

Balmain[9] has developed a theory of a dipole antenna in an anisotropic medium under quasi-static conditions, and has shown that his result could be simply rederived by applying a proper scaling to the space coordinates and the charge density. We will summarize this method and apply it to the present problem.

In a plasma with a magnetic field oriented along the Z axis, Poisson's equation is written

$$\epsilon_T \frac{\partial^2 V}{\partial x^2} + \epsilon_T \frac{\partial^2 V}{\partial y^2} + \epsilon_L \frac{\partial^2 V}{\partial z^2} = - \frac{\rho}{\epsilon_o} , \tag{34}$$

where ρ is the charge density.

Poisson's equation is elliptic when ϵ_T and ϵ_L have the same sign and hyperbolic when they have opposite sign. First we will assume that ϵ_T and ϵ_L are both positive.

The charge conservation equation is written

$$\nabla \cdot \vec{J} + j\omega\rho = o , \tag{35}$$

where $\vec{J}$ is the vector current density.

If one applies the following transformation

$$x' = \sqrt{\epsilon_L \epsilon_T}\, x, \quad y' = \sqrt{\epsilon_L \epsilon_T}\, y, \quad z' = \epsilon_T Z , \tag{36}$$

$$\text{and} \quad \rho' = \frac{\rho}{\epsilon_L \epsilon_T^2} , \tag{37}$$

equations (34) and (35), respectively, reduce to the free space formulation

$$\nabla'^2 V = -\frac{\rho'}{\epsilon_o} \tag{38}$$

and

$$\nabla' \cdot \vec{J}' + j\omega\rho' = o \ , \tag{39}$$

where the operator ∇' stands for $\frac{\partial}{\partial x'} + \frac{\partial}{\partial y'} + \frac{\partial}{\partial z'}$.

One notes that this transformation leaves the potential and the frequency invariant. Though the charge density is transformed by Eq. (37), the charge itself is also an invariant.

If we apply the space transformation (36) to the electric field $\vec{E}$ and the element of surface area $\vec{dS}$ we obtain

$$\vec{E} = -\begin{pmatrix} \partial V/\partial x \\ \partial V/\partial y \\ \partial V/\partial z \end{pmatrix} = -(m)\begin{pmatrix} \partial V/\partial x' \\ \partial V/\partial y' \\ \partial V/\partial z' \end{pmatrix} = -(m)\,\vec{E}' \ , \tag{40}$$

where $(m) = \begin{pmatrix} \sqrt{\epsilon_L \epsilon_T} & o & o \\ o & \sqrt{\epsilon_L \epsilon_T} & o \\ o & o & \epsilon_T \end{pmatrix}$ and $\vec{E}'$ is found from Eq. (38),

$$\vec{dS} = \begin{pmatrix} \partial y \partial z \\ \partial z \partial x \\ \partial x \partial y \end{pmatrix} = (n)\begin{pmatrix} \partial y' \partial x' \\ \partial z' \partial x' \\ \partial x' \partial y' \end{pmatrix} = (n)\,\vec{dS}' \tag{41}$$

where $(n) = \begin{pmatrix} \frac{1}{\epsilon_T \sqrt{\epsilon_L \epsilon_T}} & o & o \\ o & \frac{1}{\epsilon_T \sqrt{\epsilon_L \epsilon_T}} & o \\ o & o & \frac{1}{\epsilon_L \epsilon_T} \end{pmatrix}$.

Replacing Eqs. (40) and (41) in Eq. (32), and noting that $\vec{E}'$ and $\vec{dS}'$ are parallel we obtain

$$C_p = \frac{\epsilon_o \int_{S'} E' dS'}{V}$$

where the space transformation has also been applied to the integration boundaries, that is the surface of the electrodes.

Therefore, the impedance of a dipole immersed in a plasma is the same as the free space impedance of a new dipole obtained from the first one through the scaling law (36).

When ϵ_L and ϵ_T are both negative, the space transformation is still meaningful if the scaling equations are written

$$x' = \sqrt{(-\epsilon_L)(-\epsilon_T)}\, x, \quad y' = \sqrt{(-\epsilon_L)(-\epsilon_T)}\, y, \quad z' = (-\epsilon_T)\, z,$$

$$\text{and} \quad \rho' = \frac{-\rho}{\epsilon_L \epsilon_T^2} .$$

Then Eqs. (38) and (39) are unchanged but, since the sign of the charge has been changed, it is clear that the capacitance is negative, i.e., the reactance of the dipole is inductive.

2. Impedance of a Dipole Made of Two Flat Strips

The basic coordinate system xyz is such that the magnetic field is oriented along the z axis. However, it is convenient to use a second coordinate system xuv obtained from the first one through a rotation of angle θ around the x axis and such that the v axis is a symmetry axis for the dipole.

Balmain[9] showed that the space transformation (36) becomes

$$x' = \sqrt{\epsilon_L \epsilon_T}\, x \ ,$$

$$u' = \frac{\epsilon_T \sqrt{\epsilon_L}}{\sqrt{\epsilon_L \sin^2\theta + \epsilon_T \cos^2\theta}}\, u \ ,$$

$$v' = \sqrt{\epsilon_T}\sqrt{\epsilon_L \sin^2\theta + \epsilon_T \cos^2\theta}\, v \quad . \tag{42}$$

Application of the transformation (42) to a dipole made of two flat strips is illustrated on Fig. 23. The length of the equivalent dipole is

$$L' = \sqrt{\epsilon_T}\sqrt{\epsilon_L \sin^2\theta + \epsilon_T \cos^2\theta}\, L \ .$$

When the azimuthal angle φ varies, the equivalent strips describe an elliptical cylinder. Their separation, D', and their width, h', are consequently functions of φ.

When the magnetic field is parallel to the electrode surface, $\varphi = o$ and

$$\frac{D'}{h'} = \frac{1}{\sqrt{\epsilon_T}}\sqrt{\epsilon_L \sin^2\theta + \epsilon_T \cos^2\theta}\ \frac{D}{h} \ . \tag{43}$$

When the magnetic field makes an angle θ with the electrode surface, $\varphi = \frac{\pi}{2}$ and

$$\frac{D'}{h'} = \frac{\sqrt{\epsilon_T}}{\sqrt{\epsilon_L \sin^2\theta + \epsilon_T \cos^2\theta}}\ \frac{D}{h} \ . \tag{44}$$

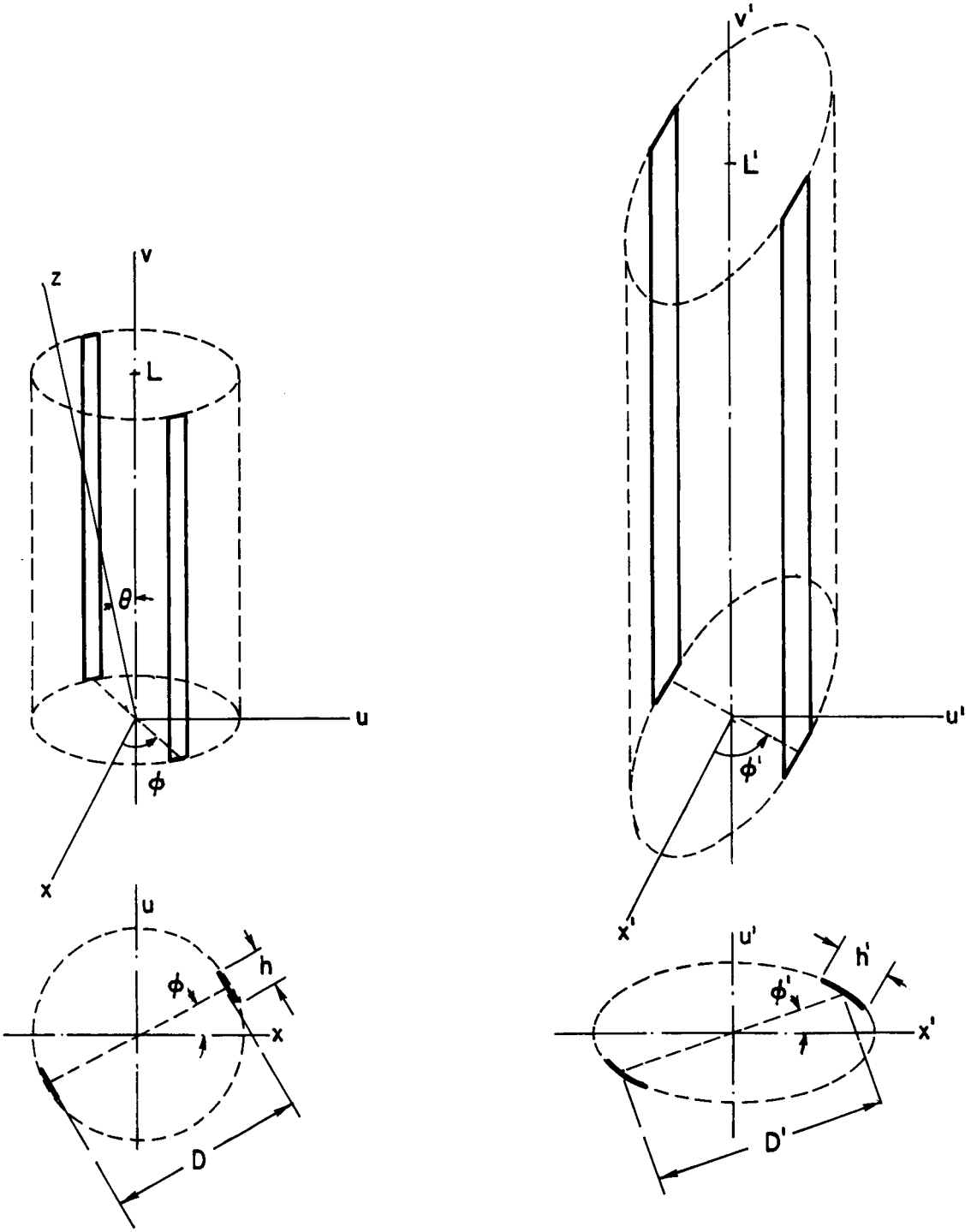

FIG. 23. GEOMETRY OF THE DIPOLE AND THE FREE SPACE EQUIVALENT CONFIGURATION.

The capacitance of two parallel strips in an homogeneous medium has been computed by Palmer[33] and some useful approximate results are given by Terman.[34] The variation of the capacitance per meter with the ratio of strip separation over strip width is given on Fig. 24.

If $\left|\frac{D'}{h'}\right| \gg 1$, the strip capacitance is given by

$$C_p = \frac{\pi \epsilon_o L'}{\ell n\ 4\ \frac{D'}{h'}} , \tag{45}$$

if $\left|\frac{D'}{h'}\right| \ll 1$, this capacitance becomes

$$C_p = \epsilon_o \frac{h'}{D'} \left[1 + \frac{D'}{\pi h'} \left(1 + \ell n\ 2\pi \frac{h'}{D'}\right)\right] L' . \tag{46}$$

Finally, the strip impedance can be written

$$Z_p = \frac{1}{j\omega C_p} ,$$

where C_p is found from one of the preceding equations, depending on the magnitude of the ratio $|D'/h'|$.

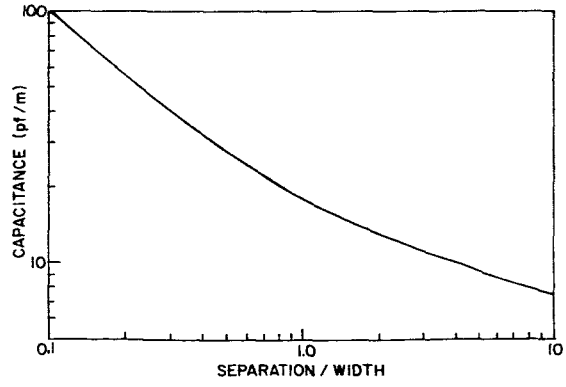

FIG. 24. CAPACITANCE OF TWO LONG PARALLEL STRIPS IN FREE SPACE.

3. Discussion

One must keep in mind that the above derivation is rigorous only if ϵ_L and ϵ_T are real and have the same sign. In the case of a plasma with one species of ion, the relative permittivities parallel and transverse to the magnetic field are given, respectively, by

$$\epsilon_L = 1 - \left(1 + \frac{M}{m}\right) \frac{\omega_{Pe}^2}{\omega^2}$$

and

$$\epsilon_T = 1 - \frac{\omega_{Pe}^2}{\omega^2 - \omega_{ce}^2} - \frac{\frac{M}{m}\omega_{Pe}^2}{\omega^2 - \left(\frac{M}{m}\right)^2 \omega_{ce}^2},$$

where m and M are the electron and ion masses, respectively, $\omega_{Pe}^2 = ne^2/\epsilon_o m$ is the electron plasma frequency and $\omega_{ce} = eB/m$ is the electron cyclotron frequency.

The regions of applicability of the scaling method are shown in Fig. 25. The impedance Z_p is capacitive in regions 1, 4 and 8, where ϵ_L and ϵ_T are both positive; it is inductive in regions 3 and 7 where ϵ_L and ϵ_T are both negative.

In regions 2, 5, 6 and 9, ϵ_T and ϵ_L have opposite signs and Laplace's equation is hyperbolic. The space transformation (36) becomes imaginary and one is left with the unusual and non-physical problem of solving Laplace's equation in free space with imaginary boundaries!

The scaling method was also used by Pyati and Weil,[35] who computed the capacitance of a biconical antenna in a magneto-ionic medium. These authors mentioned that it was possible analytically to continue the expression found for Z_p, valid in the regions where Laplace's equation is elliptic, into the regions where Laplace's equation is hyperbolic. The work of Balmain[9] also supports this conclusion.

When Laplace's equation is hyperbolic, it can be seen from Eqs. (43) and (44) that D'/h' may become imaginary. Then the

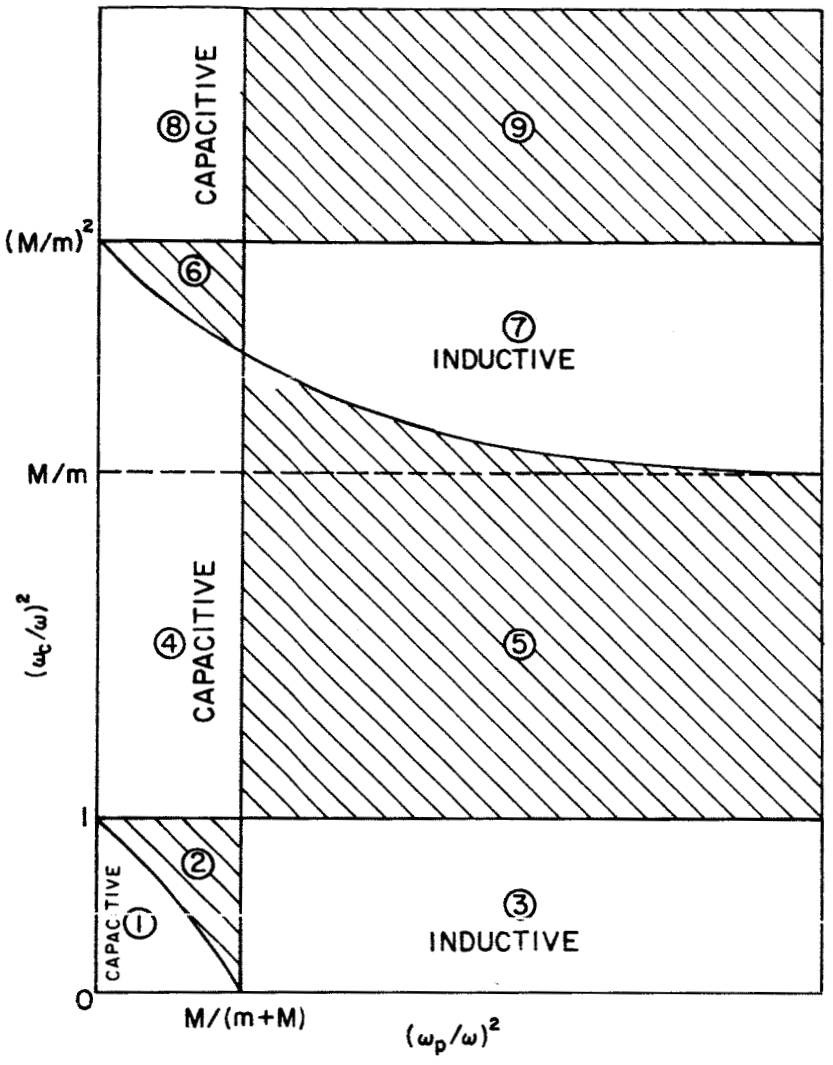

FIG. 25. REGIONS OF APPLICABILITY OF THE SCALING METHOD.

capacitance of the strips, given by Eq. (45) or (46) becomes complex and the impedance Z_p presents a real part in a lossless medium.

The physical meaning of this resistance is not well understood and the validity of this theoretical result is sometimes rejected. Balmain[9] suggests that this resistance is due to radiation. Pyati and Weil[35] and Walsh and Haddock[36] do not agree with this interpretation and mention that a quasi-static approximation is no longer valid when the wavelengths in certain propagation directions are no longer large with respect to the size of the antenna.

The determination of the impedance of an antenna in a magneto-ionic medium is very important for very low frequency reception and transmission aboard rockets and satellites. This problem has not been solved satisfactorily yet; an accurate treatment would require using the wave equation instead of Laplace's equation in the computations, but this is not mathematically feasible.

No reliable measurements of impedance have been made so far in the controversial regions of Fig. 25. Such experimentation would be very valuable; it would show if the available impedance models are valid and at least would help to understand the behavior of an antenna in a medium where Poisson's equation is hyperbolic.

4. Numerical Application

The dipole model used in the preceding computations is similar to the one used in the ionospheric experiment with the exception that a portion of space is occupied by the rocket in the latter model. The equations which were written do not represent exactly the plasma impedance of the real probe, but will give an insight into its magnitude.

We have computed the modulus of the capacitance of two flat strips for a frequency of 1.54 kc/s and for two values of the azimuthal angle, $\varphi = o$ and $\varphi = \frac{\pi}{2}$. Collisions are neglected and the range of electron density is similar to that observed during the rocket flight. The plasma is assumed to be made of ionized oxygen. The electron and ion gyrofrequencies are supposed to be, respectively, 1.45 Mc/s and 49 c/s. Such conditions are characteristic of region 7 on Fig. 25.

The results are displayed on Fig. 26. This figure is more than illustrative because it shows that the plasma capacitance is very large compared to the measured external capacitance at 1.54 kc/s. In the worst case, when $\varphi = o$, a ratio of at least 500 exists between the modulus of these two capacitances. Consequently, it is justified to assume that the plasma is a perfect conductor at the lower frequency. Therefore, if we have $Z_p \simeq 0$, we see from Fig. 22 that the impedance of the dipole consists of the internal capacitance in parallel with the sheath impedance of the strips.

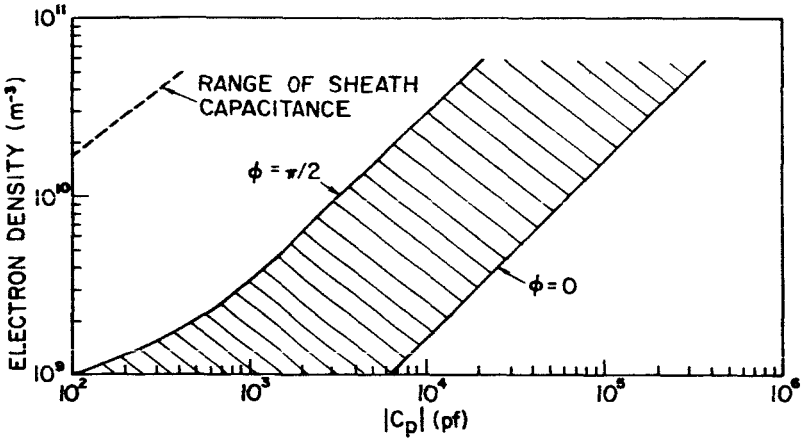

FIG. 26. MODULUS OF THE DIPOLE CAPACITANCE IN A MAGNETO-IONIC MEDIUM, FREQUENCY 1.54 KC/S.

Conclusions relative to the upper frequency, 120 kc/s, cannot be drawn because Poisson's equation is hyperbolic in region 5 of Fig. 25 and the scaling process cannot be applied with confidence.

However, the magnitude of the elements of the dielectric tensor suggests that the plasma impedance is no longer negligible at high frequency and that the corresponding data are not characteristic of the sheath impedance.

C. EFFECT OF THE PARTICLE THERMAL VELOCITY ON THE PLASMA IMPEDANCE

1. Theory

At an altitude of 200 km, the top of the trajectory, and under nighttime conditions, the electron temperature given by Johnson[37] is 700 °K. Electrons are consequently moving on helical orbits along the magnetic field direction with an average velocity of 140 km/s. Since the magnetic field makes an angle of only 30° with the rocket axis, we can roughly define a time during which an electron is interacting with the electric field of the dipole. This transit time equals the ratio of the dipole length over the electron velocity, that is roughly 10^{-5} s. In other words, an average electron travels over a distance of 100 m during one period of the 1.54 kc/s signal. Under such conditions we

may wonder if the cold plasma approximation used in the preceding computations is still valid at low frequency.

The effect of the temperature was also mentioned by Kaiser;[21] we will try to estimate its importance by using a simpler electrode configuration. We will compute the impedance of a slab of plasma limited by two parallel plates as shown on Fig. 27. A uniform ac electric field exists along the z axis and a uniform dc magnetic field is applied along the y axis. We assume that there is no collision and we neglect the collection of particles by the electrodes.

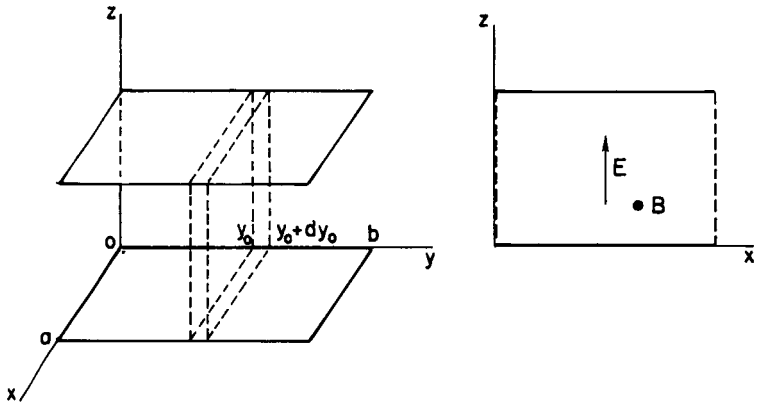

FIG. 27. THE MODEL UTILIZED IN THE COMPUTATION OF THE EFFECT OF TEMPERATURE UPON THE IMPEDANCE OF THE PLASMA.

The law of motion of a particle of charge q and mass m is written

$$m\dot{\vec{c}} = q\,(\vec{E} + \vec{c} \times \vec{B}) \ , \qquad (47)$$

where $\vec{c}$ = the velocity of the particle.

Equation (47) is equivalent to the following set

$$m\ddot{x} = - q B \dot{z} \ , \qquad (48)$$

$$m\ddot{y} = o \ ,$$

$$m\ddot{z} = q\,(E + B\dot{x}) \ . \qquad (49)$$

Integrating Eq. (48) and replaxing $\dot{x}$ in Eq. (49), we obtain

$$\ddot{z} + \omega_c^2 z = \frac{q}{m} E \ , \tag{50}$$

where $\omega_c = \frac{qB}{m}$.

If we assume that $E = E_o \cos \omega t$, the complete solution of Eq. (50) is

$$z - z_o = \frac{q}{m} \frac{E_o}{\omega_c^2 - \omega^2} \cos \omega t + A \cos (\omega_c t + \phi) \ , \tag{51}$$

where A and ϕ are two integration constants and z_o is the value of z at $y = o$.

The particle which is at position $y = y_o$ at time t was at position $y = o$ at time $t - (y_o/v)$, v being the velocity of the particle along the z axis. We can determine A and ϕ by the boundary conditions $z = z_o$ and $\dot{z} = \dot{z}_o$ at $y = o$.

These conditions can be written

$$\frac{q}{m} \frac{E_o}{\omega_c^2 - \omega^2} \cos \left(\omega t - \frac{\omega y_o}{v} \right) + A \cos \left(\omega_c t - \frac{\omega_c y_o}{v} + \phi \right) = o$$

$$- \frac{q}{m} \frac{E_o}{\omega_c^2 - \omega^2} \omega \sin \left(\omega t - \frac{\omega y_o}{v} \right) - A \omega_c \sin \left(\omega_c t - \frac{\omega_c y_o}{v} + \phi \right) = \dot{z}_o \ ,$$

from which we obtain the integration constants,

$$A = - \frac{q}{m} \frac{E_o}{\omega_c^2 - \omega^2} \cos \left(\omega t - \frac{\omega y_o}{v} \right) \sqrt{1 + X^2}$$

and

$$\phi = \text{Arc tg} X + \frac{\omega_c y_o}{v} - \omega_c t \ ,$$

where

$$X = \frac{\omega}{\omega_c} \operatorname{tg}\left(\omega t - \frac{\omega y_o}{v}\right) + \frac{\dot{z}_o}{E_o}\frac{m}{q}\frac{\omega_c^2 - \omega^2}{\omega_c}\frac{1}{\cos\left(\omega t - \frac{\omega y_o}{v}\right)}$$

Then taking the derivative of Eq. (47) we obtain

$$\dot{z} = \frac{q}{m}\frac{E_o}{\omega_c^2 - \omega^2}\left[-\omega \sin \omega t + \omega_c \cos\left(\omega t - \frac{\omega y_o}{v}\right)\sqrt{1 + X^2}\sin\left(\text{Arc tg } X + \frac{\omega_c y_o}{v}\right)\right],$$

or

$$\dot{z} = \frac{q}{m}\frac{E_o}{\omega_c^2 - \omega^2}\left[-\omega \sin \omega t + \omega_c X \cos\left(\omega t - \frac{\omega y_o}{v}\right)\cos\frac{\omega_c y_o}{v} + \omega_c \cos\left(\omega t - \frac{\omega y_o}{v}\right)\sin\frac{\omega_c y_o}{v}\right]$$

Putting $\mu = \frac{\omega_c}{\omega}$ and replacing for X, we obtain

$$\dot{z} = \frac{q}{m}\frac{E_o}{1 - \mu^2}\frac{1}{\omega}\left[\sin \omega t - \sin\left(\omega t - \frac{\omega y_o}{v}\right)\cos\frac{\omega_c y_o}{v} - \mu \cos\left(\omega t - \frac{\omega y_o}{v}\right)\sin\frac{\omega_c y_o}{v}\right] + \dot{z}_o \cos\frac{\omega_c y_o}{v}$$

or

$$\dot{z} = \frac{q}{m}\frac{E_o}{1 - \mu^2}\frac{1}{\omega}\left\{\sin \omega t - \frac{1 + \mu}{2}\sin\left[\omega t - (1-\mu)\frac{\omega y_o}{v}\right] - \frac{1 - \mu}{2}\sin\left[\omega t - (1+\mu)\frac{\omega y_o}{v}\right]\right\} + \dot{z}_o \cos\frac{\omega_c y_o}{v} \quad . \qquad (52)$$

The last term can be dropped because it gives no contribution at frequency ω; it just represents the projection along the z axis of the circular motion of a charged particle in a magnetic field.

The total current along the z axis due to a beam of particles of velocity v is obtained from Eq. (52) through the following integration

$$I = nqa \int_o^b \dot{z}\, dy$$

or

$$I = \epsilon_o \frac{\omega_p^2}{\omega} \frac{E_o}{1 - \mu^2} a \int_o^b \left\{ \sin \omega t - \frac{1 + \mu}{2} \sin \left[\omega t - (1-\mu) \frac{\omega y}{v} \right] \right.$$

$$\left. - \frac{1 - \mu}{2} \sin \left[\omega t - (1 + \mu) \frac{\omega y_o}{v} \right] \right\} dy \ , \qquad (53)$$

where $\omega_p^2 = \frac{nq^2}{m\epsilon_o}$, a and b being, respectively, the width and the length of the plates.

After integration of Eq. (53) and some transformations, the current density in the z direction $j = \frac{I}{ab}$ is found to be

$$j = \epsilon_o \frac{\omega_p^2}{\omega} \frac{E_o}{1 - \mu^2} \left\{ \sin \omega t \left[1 - \frac{1 + \mu}{2} \frac{\sin (1 - \mu)u}{(1 - \mu)u} - \frac{1 - \mu}{2} \frac{\sin (1 + \mu)u}{(1 + \mu)u} \right] \right.$$

$$\left. + \cos \omega t \left[\frac{1 + \mu^2}{1 - \mu^2} \frac{1}{u} - \frac{1 + \mu}{2} \frac{\cos (1 - \mu)u}{(1 - \mu)u} - \frac{1 - \mu}{2} \frac{\cos (1 + \mu)u}{(1 + \mu)u} \right] \right\} \ ,$$

where $u = \frac{\omega b}{v}$.

These calculations are relative to a beam of particles which has a velocity v along z axis. We must now average this result over the velocity distribution function of the particles. For simplicity we assume a monoenergetic and isotropic distribution function as shown on Fig. 28a.

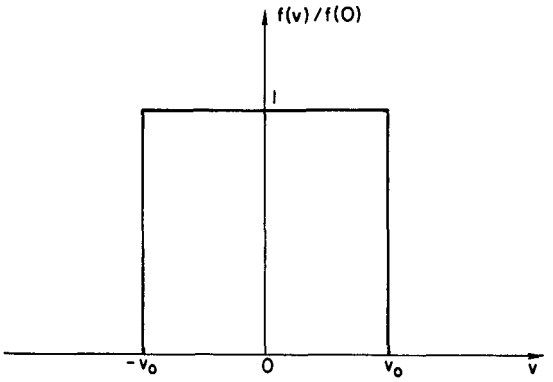

a. Monoenergetic and isotropic distribution function

Fig. 28a. Garad
65 percent

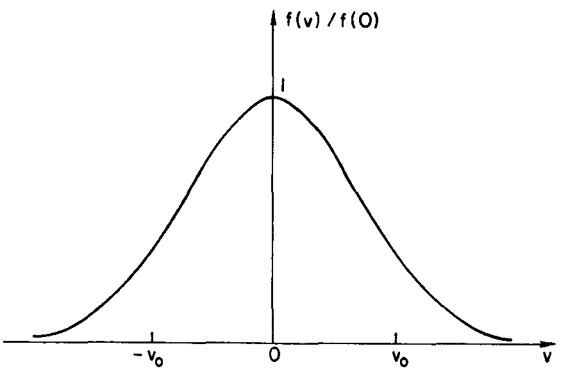

b. Maxwellian distribution function

FIG. 28. TWO KINDS OF VELOCITY DISTRIBUTION FUNCTION.

$$J = \frac{1}{v_o} \int_o^{v_o} j \, dv \ ,$$

where v_o is the velocity of the particles. Putting $\frac{\omega b}{v_o} = \tau$, we obtain

$$J = \epsilon_o \frac{\omega_p^2}{\omega} E_o \frac{\tau}{4} \left[\sin \omega t \left\{ \frac{4}{(1 - \mu^2)\tau} \right.\right.$$

$$- \frac{\sin [(1 + \mu)\tau]}{(1 + \mu)^2 \tau^2} - \frac{\cos [(1 + \mu)\tau]}{(1 + \mu)\tau} - \text{Si } [(1 + \mu)\tau] + \frac{\pi}{2}$$

$$\left. - \frac{\sin [(1 - \mu)\tau]}{(1 - \mu)^2 \tau^2} - \frac{\cos [(1 - \mu)\tau]}{(1 - \mu)\tau} - \text{Si } [(1 - \mu)\tau] + \frac{\pi}{2} \right\}$$

$$+ \cos \omega t \left\{ \frac{1 + \mu^2}{(1 - \mu^2)^2} \frac{2}{\tau^2} \right.$$

$$- \frac{\cos [(1 + \mu)\tau]}{(1 + \mu)^2 \tau^2} + \frac{\sin [(1 + \mu)\tau]}{(1 + \mu)\tau} - \text{Ci } [(1 + \mu)\tau]$$

$$\left.\left. - \frac{\cos [(1 - \mu)\tau]}{(1 - \mu)^2 \tau^2} + \frac{\sin [(1 - \mu)\tau]}{(1 - \mu)\tau} - \text{Ci } [(1 - \mu)\tau] \right\} \right]$$

The total current density will be found by adding the contribution of each species of particles and the vacuum displacement current. Then the equivalent relative permittivity of the medium is

$$\epsilon_T = 1 - \sum \frac{\omega_p^2}{\omega^2} (\alpha_T + j\beta_T) , \qquad (54)$$

where the summation sign indicates that one must add the effect of all species of particles and where

$$\alpha_T = \frac{1}{1-\mu^2} - \frac{\tau}{4}\left\{\frac{\sin(1+\mu)\tau}{(1+\mu)^2\tau^2} + \frac{\cos(1+\mu)\tau}{(1+\mu)\tau} + \mathrm{Si}\left[(1+\mu)\tau\right] - \frac{\pi}{2}\right.$$

$$\left. + \frac{\sin(1-\mu)\tau}{(1-\mu)^2\tau^2} + \frac{\cos(1-\mu)\tau}{(1-\mu)\tau} + \mathrm{Si}\left[(1-\mu)\tau\right] - \frac{\pi}{2}\right\} \tag{55}$$

and

$$\beta_T = \frac{1+\mu^2}{(1-\mu^2)^2}\frac{1}{2\tau} - \frac{\tau}{4}\left\{\frac{\cos(1+\mu)\tau}{(1+\mu)^2\tau^2} - \frac{\sin(1+\mu)\tau}{(1+\mu)\tau} + \mathrm{Ci}\left[(1+\mu)\tau\right]\right.$$

$$\left. + \frac{\cos(1-\mu)\tau}{(1-\mu)^2\tau^2} - \frac{\sin(1-\mu)\tau}{(1-\mu)\tau} + \mathrm{Ci}\left[(1-\mu)\tau\right]\right\} \tag{56}$$

When the magnetic field is parallel to the electric field, or when no magnetic field is present, the relative permittivity is given by

$$\epsilon_L = 1 - \sum \frac{\omega_p^2}{\omega^2}\left(\alpha_L + j\beta_L\right), \tag{57}$$

where α_L and β_L are given by Eqs. (55) and (56) where μ has been put equal to zero, that is

$$\alpha_L = 1 - \frac{1}{2}\left[\frac{\sin\tau}{\tau} + \cos\tau + \tau\,\mathrm{Si}(\tau) - \tau\frac{\pi}{2}\right] \tag{58}$$

and

$$\beta_L = \frac{1}{2}\left[\frac{1-\cos\tau}{\tau} + \sin\tau - \tau\,\mathrm{Ci}(\tau)\right] \tag{59}$$

One sees that the equivalent permittivity of the plasma is complex; the medium appears to be lossy not because of the collisions, which we neglected, but because the particles have increased their kinetic energy during their interaction with the electric field and have taken that energy away from the system.

A plot of Eqs. (58) and (59) is made on Fig. 29. It can be seen that when τ goes to infinity, that is, when the product of the transit time by the frequency is large, β_L goes to zero and α_L goes to 1, then Eq. (57) yields the permittivity of a cold plasma.

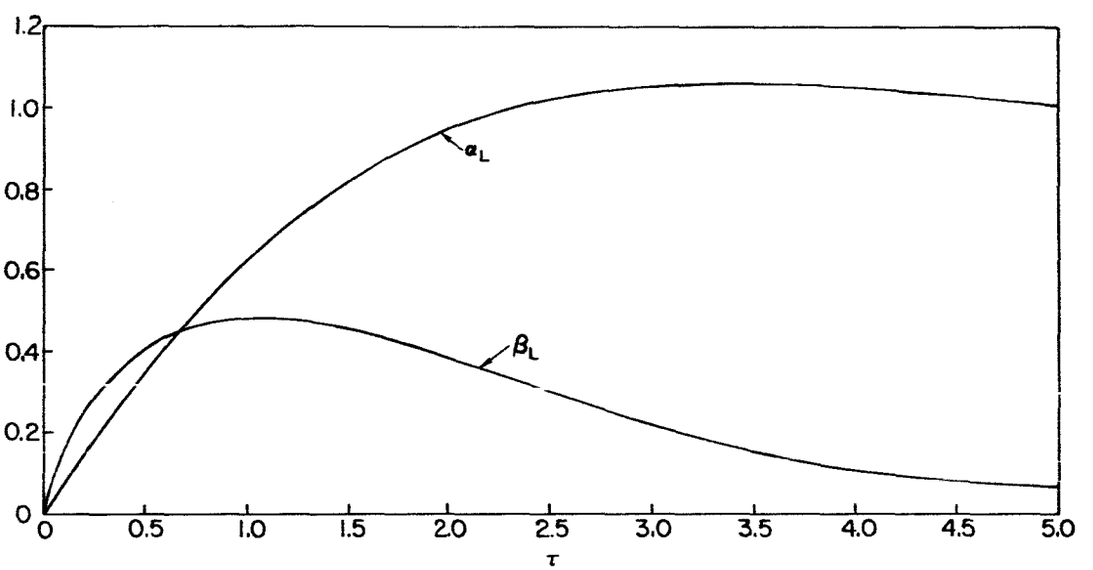

FIG. 29. PLOT OF THE QUANTITIES α_L AND β_L, MONOENERGETIC DISTRIBUTION.

In order to check the importance of the shape of the velocity distribution function on these results, we have also considered the case of a Maxwellian distribution function shown on Fig. 28b. This problem was solved with a computer by decomposing this distribution function into a large number of monoenergetic and isotropic distribution functions and by adding the contribution of each elementary group of particles.

The variations of the quantities α_L and β_L with τ for a Maxwellian distribution function are shown in Fig. 30. The difference between these curves and those displayed on Fig. 29 is very small.

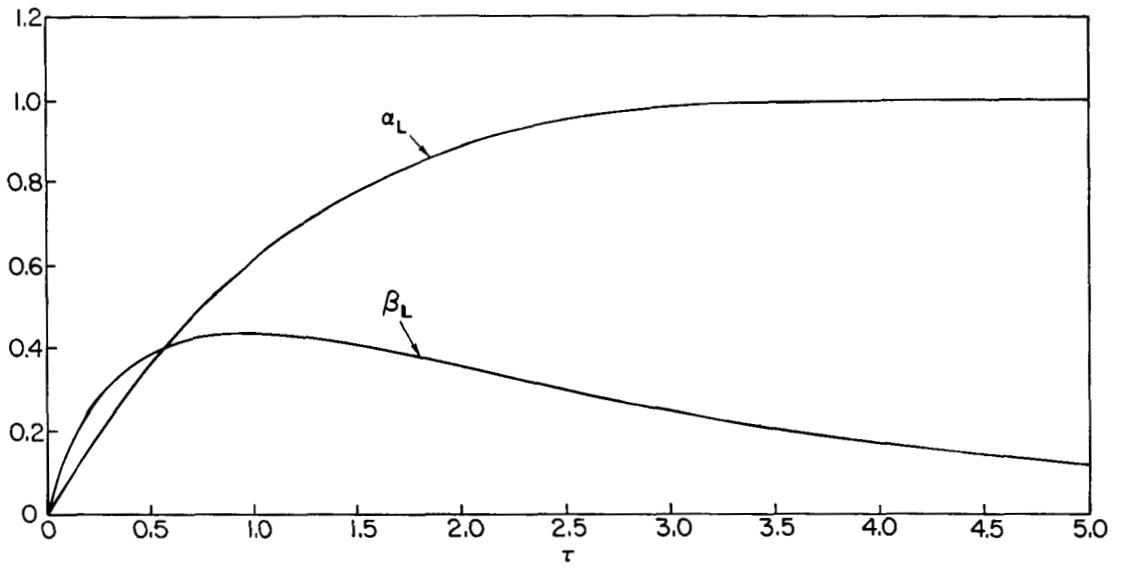

FIG. 30. PLOT OF THE QUANTITIES α_L AND β_L, MAXWELLIAN DISTRIBUTION.

2. Numerical Application

We will try now to evaluate Eqs. (54) and (57), using the features of the plasma corresponding to the top of the trajectory. We assume that the plasma is made of ionized oxygen and that its temperature equals 700 °K. The frequency is 1.54 kc/s and the length of interaction between the electric field and the particles is 1 m.

The electron parameters are

$$\omega_{pe} = 2\pi \times 10^6 \ s^{-1} ,$$

$$\omega_{ce} = 2\pi \times 1.45 \times 10^6 \ s^{-1} ,$$

$$\mu_e = \frac{1.45 \times 10^6}{1.54 \times 10^3} \simeq 10^3 ,$$

$$v_{oe} = 140 \times 10^3 \text{ m/s}$$

and

$$\tau_e = 2\pi \times 1.54 \times 10^3 \frac{1}{140 \times 10^3} \simeq 0.07 .$$

The ion parameters are

$$\omega_{pi} = 2\pi \times 5.8 \times 10^3 \text{ s}^{-1} ,$$

$$\omega_{ci} = 2\pi \times 49 \text{ s}^{-1} ,$$

$$\mu_i = \frac{49}{1.54 \times 10^3} \simeq 3.2 \times 10^{-2} ,$$

$$v_{oi} = 820 \text{ m/s}$$

and

$$\tau_i = 2\pi \times 1.54 \times 10^3 \frac{1}{820} \simeq 12 .$$

Putting these quantities into Eqs. (54) - (59) one finds

$$\epsilon_T \simeq 1 - \frac{\omega_{pe}^2}{\omega^2 - \omega_{ce}^2} - \frac{\omega_{pi}^2}{\omega^2 - \omega_{ci}^2}$$

and

$$\epsilon_L \simeq 1 - \frac{\omega_{pe}^2}{\omega^2} (0.1 + j\, 0.2) .$$

In other words the transit time effect has little influence on ϵ_T but perturbs seriously ϵ_L.

Effectively, the longitudinal dielectric constant appears to be that of a lossy medium and its modulus is approximately 5 times smaller than its value computed from the cold plasma theory. This

discrepancy is sizeable but not large enough to invalidate the conclusion of the preceding paragraph and we can consider that, under the less favorable conditions, the plasma impedance is of the order of 1 percent of the sheath impedance, at 1.54 kc/s.

In fact, because of the edge effect, the electric field acting on the particles is not varying abruptly from zero to a constant value; this lengthens the interaction time between the particles and the field and yields a transit time effect less important than that which was computed above.

D. THE IMPEDANCE OF THE SHEATH

1. The Modulation of the Data

We will now consider the low frequency data for further numerical comparisons. They represent mainly the sheath admittance because the plasma contribution has been shown to be negligible. Figure 31, due to Orsak et al,[18] displays the components of the admittance as a function of the azimuthal angle of the dipole. It shows that the capacitance and the conductance are modulated at twice the spin rate of the rocket.

Only 5 samples were transmitted for each revolution of the rocket around its axis and the curves are the result of the superposition of the data received during 8 consecutive revolutions. These curves correspond to the top of the trajectory where the rocket altitude is stationary and the plasma parameters are relatively constant during several revolutions. Elsewhere on the trajectory it is not possible to separate the effect of the rocket spin from that of the electron density variation.

The directions of the velocity and magnetic field components normal to the rocket axis are shown. It is not possible to determine what factor is responsible for the modulation because the admittance shows a maximum in the velocity direction and a minimum in the magnetic field direction.

The size of the sheath and the floating potential are perturbed when the strip is in the wake of the rocket, because the transverse velocity of the vehicle has the same order of magnitude as the ion

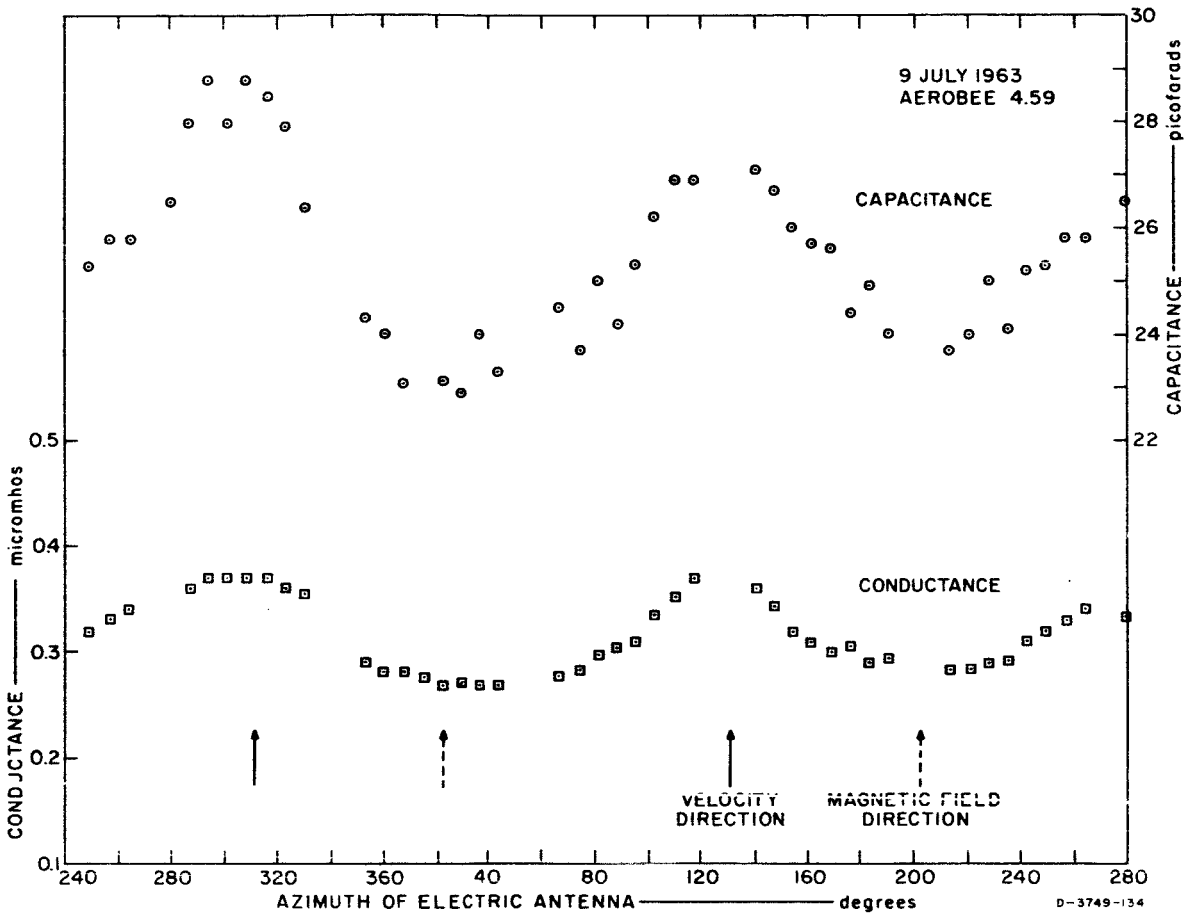

FIG. 31. ROCKET SPIN MODULATION OF IMPEDANCE AT THE TOP OF THE TRAJECTORY, FREQUENCY 1.54 kc/s. (Courtesy of L. E. Orsak, L. H. Rorden, G. B. Carpenter and B. P. Ficklin, Stanford Research Institute, Final Rept., Contract NASr-49(01), Jan 1965.)

thermal velocity. Therefore we can assume that the most accurate reading of the dipole admittance is made when the vector velocity is parallel to the surface of the electrodes. Then, the motion of the ions in the vicinity of the strips and the size of the sheath are the same as if the rocket were at rest. Consequently, for comparisons with theoretical predictions, we consider that the dipole conductance and capacitance are respectively 0.29 μmhos and 24 pf.

2. The Probe Admittance

Using Eqs. (8) and (9), the sheath conductance is written

$$G_s = Ane\sqrt{\frac{e}{2\pi m V_e}} \exp \frac{V_f}{V_e} , \qquad (60)$$

where G_s, the conductance of one strip, equals 0.58 μmhos.

The surface area, A, equals 271 cm^2. At an altitude of 200 km, the top of the trajectory, a propagation method gave $n = 1.7 \times 10^{10}$ m^{-3}. The electron temperature, measured with a Langmuir probe was 800 °K, which corresponds to $V_e = 0.07$ volts, and is in good agreement with the data given by Johnson.[37]

Putting these numerical values into Eq. (60) gives for the floating potential

$$V_f = - 4.30\ V_e = - 0.31 \text{ volts} ,$$

which compares favorably with Bohm's prediction, $V_f = - 4.23\ V_e$, where it is assumed that the ambient plasma consists of ionized oxygen.

The electromotive force induced by the earth's magnetic field in one strip, which varies from 0 to 7 m-volt, is absolutely negligible with respect to the probe floating potential.

If we assume that V_f/V_e is a constant and if we know V_e, Eq. (60) can give the electron density profile. We assume that the temperature vs altitude is given by Fig. 32. This curve is given by Johnson[37] and has been normalized to give a temperature of 800 °K at an altitude of 200 km.

We used the data of Fig. 18 to plot the electron density profile on Fig. 33. The profile was normalized in such a way that a dipole conductance of 0.29 μmhos corresponds to an electron density of 1.7×10^{10} m^{-3}.

The discrepancies between the ascent and the descent data and the subsequent inaccuracy of the density profile have several origins. The modulation of the data due to the rocket wake can cause

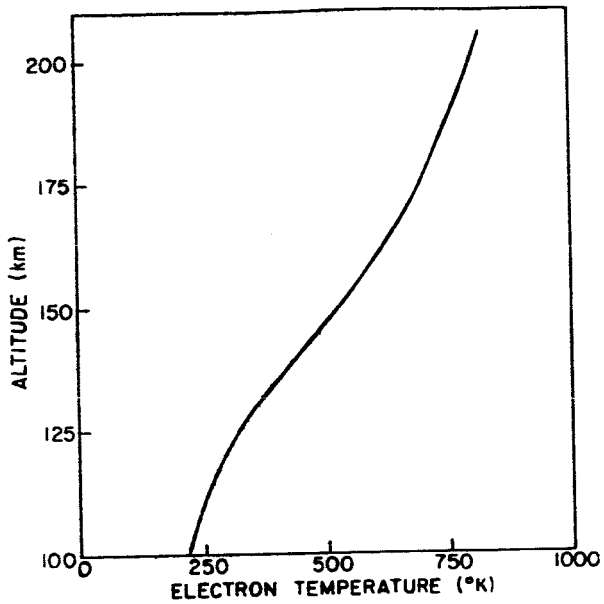

FIG. 32. TEMPERATURE PROFILE ASSUMED IN THE DERIVATION OF THE ELECTRON DENSITY.

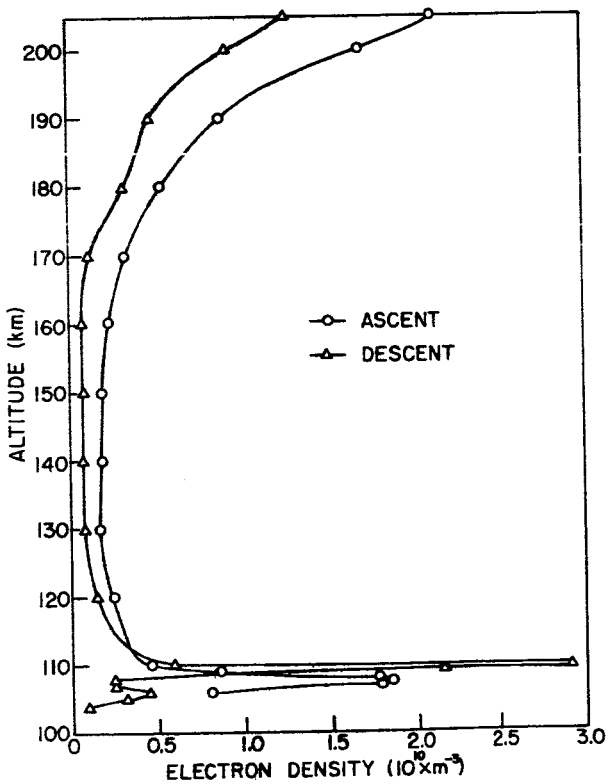

FIG. 33. PLOT OF THE ELECTRON DENSITY DETERMINED FROM THE CONDUCTANCE MEASUREMENTS AT 1.54 kc/s.

a relative error as high as 30 percent at the top of the trajectory; this error is larger during the descent than during the ascent since the velocity component normal to the rocket axis was increasing with time. The nose cone was contaminated, or heated, during the initial part of the flight, and this resulted in an increase of the conductance; this effect, which dissipated during the rest of the flight, could explain why the conductance is generally higher during the ascent than during the descent. Space and time variations of the ionospheric parameters may also explain part of the discrepancies. Finally, the temperature model that we used could be inadequate. An attempt was made during the flight to measure the electron temperature with a Langmuir probe, but no information was obtained, except at the top of the trajectory, because the rocket was traveling a distance of the order of 1 km during the time required for sweeping the probe potential.

3. The Probe Capacitance

We will now attempt to compare the predicted value of the dipole capacitance with that measured at 200 km.

The plasma is an excellent conductor and the sheath capacitance of one strip is equivalent to twice the free space capacitance of the strip and its image with respect to the sheath edge, as shown on Fig. 31.

This equivalence is not perfect because the strip is not isolated in space but attached to the nosecone; this will somewhat increase the value of the capacitance, but not drastically, because the rocket skin, made of fiber glass, is only 1.6 mm thick. This model implies also that the curvature of the rocket skin can be neglected; in fact, we can use the planar approximation to compute the thickness of the sheath, $d = \lambda_D/\gamma$, because the ratio of the rocket radius over the Debye length is larger than 10. The computed value of λ_D is 1.5 cm. As for γ, we read the average of Models I, II and III on Fig. 7, which is 0.412 for ionized oxygen. Then the sheath thickness is estimated to be 3.5 cm and the separation between the strip and its image is 7 cm.

The width of the strip being 2.54 cm, one can readily check on Fig. 24 that the capacitance of one probe and its image equals 10.8 pf. This is also the total sheath capacitance of a dipole made of two identical probes in series.

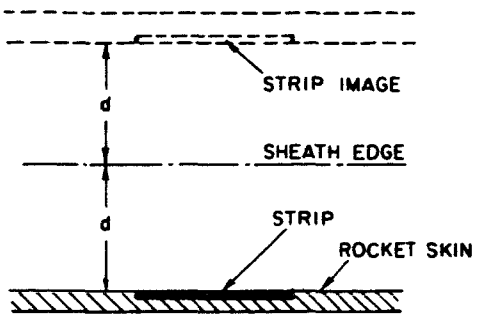

FIG. 34. SECTION OF ONE STRIP AND ITS ELECTRIC IMAGE WITH RESPECT TO THE SHEATH EDGE.

To that sheath capacitance one must add the internal capacitance, which has been estimated previously to be $C_i = 11 \pm 4$ pf, in order to find the total capacitance of the dipole

$$C = C_s + C_i = 21.8 \pm 4 \text{ pf} ,$$

which agrees fairly well with the measured value, 24 pf.

The cause of errors in the interpretation of the capacitance data are the same as those mentioned for the conductance. Moreover, the fact that C_i is not precisely known adds also to the uncertainty of the sheath capacitance.

E. DISCUSSION

The measurements of the dipole impedance at low frequency can be explained by the contribution of the sheath alone. But the interpretation of these data has been complicated by the singular geometry of the probe and the lack of information on the electron temperature. Computing the part of the impedance due to the magnetized plasma is not straightforward even for simple geometries. The effect of the particle thermal motions must also be taken into account. Consequently, the working frequency must be low enough for the plasma impedance to be negligible with respect to the sheath impedance. In the present case a frequency of the order of 1 kc/s seemed adequate.

Working at low frequency can make the sheath susceptance negligible but it seems preferable to limit the measurements to the conductance and be sure that the plasma impedance is negligible. The conductance

depends less on the geometry than the susceptance and the interpretation of the capacitance measurements can be complicated by the presence of an internal capacitance which is not well defined.

The conductance measurements should be made with a probe biased to a constant positive potential with respect to the carrying vehicle. The biasing potential can be of the order of magnitude of the electron potential, say 0.05 volt in the lower ionosphere. This insures that the velocity distribution function of the collected electrons is more closely represented by a Maxwellian function. Furthermore, the electron temperature can be obtained from the ratio of the conductance over the dc collected current.

One must not expect a direct determination of the electron density from the conductance because the latter varies exponentially with the probe potential and an accurate measurement of this potential cannot be made. However, an electron density profile can be drawn if the probe has been calibrated by an independent measurement.

The data of the present experiment are perturbed by the wake of the rocket. Therefore, the VLF impedance probe seems to be an interesting tool for studying the deformation of the sheath due to the wake. If such an experiment were to be performed, it would be more informative to measure the impedance of one strip only with respect to the rocket body acting as an electric ground, instead of the impedance of two strips in series. The modulation due to the spin would be more important and the data could be interpreted more easily. If the wake perturbation must be avoided, however, the location of the probe should be changed. A cylindrical dipole mounted on the top of the nosecone would give data less influenced by the wake of the rocket. It would also eliminate the internal capacitance.

V. CONCLUSION

If the low-frequency impedance is measured between two electrodes, two extreme conditions can be distinguished: that in which the impedance of the plasma substantially unperturbed by the probe dominates, and that in which local space-charge sheaths around the electrodes constitute the most important impedance components. Which of these is approached in an experimental situation will depend on the electrode sizes and separation, and on the measuring frequency. The impedance of the sheath becomes negligible with respect to the impedance of the plasma when the frequency and the distance between the electrodes become sufficiently large.

The former case can be handled using the effective plasma permittivity concept. The theory is relatively simple in an isotropic and homogeneous medium, but becomes more complicated when the medium is not isotropic, for example, at very low frequency in a magnetoplasma. Moreover we have shown that the cold plasma approximation is no longer valid when the distance traveled by the electrons during one period of the ac signal is large with respect to the size of the probe. Consequently, the plasma impedance probe must be used at a frequency well above the electron cyclotron and plasma frequencies; this technique can be used with more confidence over a wider range of frequency if the perturbing effect of the sheath is reduced by biasing the potential of the probe to the space potential.

This kind of measurement yields the electron density. It is, however, recommended that more data be gathered in the frequency domains where Poisson's equation is hyperbolic, because the physical behavior of an antenna under such conditions is not well understood yet and is the subject of controversy.

Such an experiment could be realized on a rocket at a frequency sufficiently high that the ion response to the ac field, the collisions and the electron thermal velocity could be neglected. If the working frequency is chosen to be 2 Mc/s, the ratio $(\omega_c/\omega)^2$ will be approximately constant during the entire flight and equal to 0.5.

Let us assume that the electron density increases monotonically from zero to about 10^{11} m^{-3} at the top of the trajectory. Then the point corresponding to the working conditions in the frequency domain will move on a horizontal line from the left to the right and will reach an abscissa equal roughly to 1.5. This is illustrated in Fig. 35, which is similar to Fig. 25, except that now we neglect the effect of the ions. The antenna impedance will be capacitive in region 1 and inductive in region 3. It will be the most interesting to observe its behavior in region 2.

The case where the impedance of the sheath is dominant has been the primary topic of this study. A simplified theory of the sheath admittance was developed and checked with results to a reasonable accuracy in the laboratory. As expected, the sheath admittance is frequency independent. At floating potential, these measurements can provide continuous relative information about the electron density. One should be aware that an absolute determination of the electron density requires that the floating potential be known with accuracy, and that the electron velocity distribution function be Maxwellian up to energies corresponding to the floating potential. Both requirements are not always satisfied. However, one can consider that the velocity distribution function of the electrons collected by the probe is more closely represented by a Maxwellian function if the potential of the probe is slightly biased toward the space potential. Furthermore,

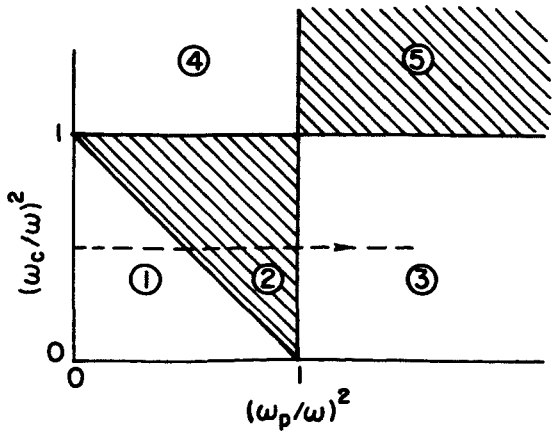

FIG. 35. THE FREQUENCY DOMAIN.

with a biased probe, an absolute estimate of the electron temperature can be made from the knowledge of the ac conductance and the dc collected current.

The interpretation of the low frequency data of the rocket experiment was complicated by the probe geometry, the spin-modulation of the data, and the lack of information about the temperature. In a new experiment it would be preferable to mount a conventional cylindrical dipole on the top of the nosecone; this would eliminate the wake effect due to the rocket body and the internal capacitance. On the other hand, if the effect of the wake on the sheath must be studied, the present geometry should be preserved but the impedance of only one strip with respect to the rocket body should be measured.

Since the wake is a perturbing factor in a number of other experiments performed aboard rockets and satellites, we suggest that a systematic study be made of this phenomenon. The size of the wake depends on the temperature of the neutrals and ions (the electrons which have a lighter mass follow the ions, in order to keep the medium neutral). Therefore, by studying the wake, one can, in principle, obtain information about the ion and neutral temperature.

A simple experiment could be realized in the following manner. An insulating rod, mounted perpendicularly to the rocket axis supports a number of equally spaced probes, as shown in Fig. 36. These probes are negatively biased and collect the ion saturation current, which is proportional to the local ion density. The rocket is generally spinning around its axis and this configuration will allow the ion density profile in the wake to be measured.

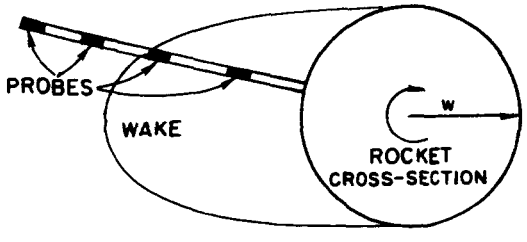

FIG. 36. EXPERIMENTAL STUDY OF THE WAKE.

An order of magnitude of the size of the wake is given by Dw/v where D is the rocket diameter, w is the rocket transverse velocity and v is the gas thermal velocity.

This experiment, combined with measurements of the plasma impedance under hyperbolic conditions, will provide information about the two major perturbing factors of the sheath impedance measurement technique.

However, the investigation made so far allows us to draw these final conclusions. The unique advantage of the sheath impedance probe lies in the fact that instantaneous and continuous measurements of the electron density and temperature can be made with a probe kept at a fixed potential. In contrast with the Langmuir probe and the resonance probe, the impedance probe requires no sweeping. It is particularly suitable for continuous measurement in time-varying plasmas and for space applications. It can be a significant tool in the study of the lower ionosphere, where steep gradients of electron density are observed, and where the collisions are frequent enough to keep the electron velocity distribution function approximately Maxwellian.

REFERENCES

1. G. Breit and M. A. Tuve, A Test of the Existence of the Conducting Layer, Physical Review, Vol. 28, No. 3, 554-75, (1926).

2. J. C. Seddon, Propagation Measurements in the Ionosphere with the Aid of Rockets, J. Geophys. Res., Vol. 58, No. 3, 323-335 (1953).

3. I. Langmuir and H. Mott-Smith, Studies of Electric Discharges in Gases at Low Pressures, General Electric Review, No. 27, 616-23, 762-71, 810-20 (1924).

4. W. R. Hoegy and L. H. Brace, The Dumbbell Electrostatic Ionosphere Probe: Theoretical Aspects, University of Michigan, Space Physics Research Laboratory, Scientific Report JS-1 (1961).

5. R. T. Bettinger, An In Situ Probe System for the Measurement of Ionospheric Parameters, University of Maryland, Department of Physics and Astronomy, Technical Report No. 277 (1964).

6. K. Takayama, H. Ikegami and S. Miyasaki, Plasma Resonance in a Radio Frequency Probe, Phys. Rev. Letters, Vol. 5, No. 6, 238-40 (1960).

7. R. S. Harp and F. W. Crawford, Characteristics of the Plasma Resonance Probe, J. Applied Phys., Vol. 35, No. 12, 3436-46 (1964).

8. J. A. Fejer, Interaction of an Antenna with a Hot Plasma and the Theory of Resonance Probes, Radio Science, Vol. 68D, No. 11, 1171-76 (1964).

9. K. G. Balmain, The Impedance of a Short Dipole Antenna in a Magnetoplasma, IEEE Trans. Ant. & Prop., Vol. AP-12, No. 5, 605-17 (1964).

10. W. E. Blair, The Driving-Point Impedance of an Electrically Short Cylindrical Antenna in the Ionosphere, University of New Mexico, Engineering Experiment Station, Tech. Rept. EE-109 (1964).

11. J. A. Kane, J. E. Jackson and H. A. Whale, The Simultaneous Measurement of Ionospheric Electron Densities by CW Propagation and RF Impedance Probe Techniques, NASA Tech. Note D-1098 (1961).

12. P. E. Crouse, Method for Obtaining Electron Density Profiles from Capacitive Ionospheric Rocket Probes, Pennsylvania State University Ionosphere Research Laboratory, Report No. 208 (1964).

13. R. F. Mlodnosky and O. K. Garriott, The VLF Admittance of a Dipole in the Lower Ionosphere, Proc. of the International Conference on the Ionosphere, Adlard and Son Ltd., Bartholomew Press, Dorking England, 484-91 (1963).

14. R. Grard, The Sheath Capacitance at VLF of a Metallic Body Moving in the Ionosphere, Stanford University, Presented at the Meeting on Direct Aeronomic Measurement in the Lower Ionosphere, University of Illinois (1963).

15. F. W. Crawford and R. F. Mlodnosky, Langmuir Probe Response to Periodic Waveforms, J. Geophys. Res., Vol. 69, No. 13, 2765-74 (1964).

16. R. Jastrow and C. A. Pearse, Atmospheric Drag on the Satellite, J. Geophys. Res., Vol. 62, No. 3, 413-24 (1957).

17. Ya. L. Al'pert, A. V. Gurevich and L. P. Pitaevskii, Effects Produced by an Artificial Satellite Rapidly Moving in the Ionosphere or in Interplanetary Medium, Soviet Phys. Uspekhi, Vol. 6, No. 1, 13-46 (1963).

18. L. E. Orsak, L. H. Rorden, G. B. Carpenter and B. P. Ficklin, VLF Propagation and Noise in the Ionosphere Observed by Sounding Rockets, Stanford Research Institute, Final Rept. Contract NASr-49(01), Jan. (1965).

19. D. Bohm, E. H. S. Burhop and H. S. W. Massey, "The Use of Probes for Plasma Exploration in Strong Magnetic Fields," The Characteristics of Electrical Discharges in Magnetic Fields, A. Guthrie and R. K. Wakerling, eds., McGraw-Hill, Inc. (1949).

20. H. S. Butler and G. S. Kino, Plasma Sheath Formation by rf Fields, Phys. of Fluids, Vol. 6, No. 9, 1346-55 (1963).

21. T. R. Kaiser, The Admittance of an Electric Dipole in a Magneto-Ionic Environment, Planet. & Space Sci., Vol. 9, 639-57 (1962).

22. S. A. Self, Exact Solution of the Collisionless Plasma Sheath Equation, Phys. of Fluids, Vol. 6, No. 12, 1762-68 (1963).

23. J. V. Parker, Collisionless Plasma-Sheath in Cylindrical Geometry, Phys. of Fluids, Vol. 6, No. 11, 1657-58 (1963).

24. Langmuir, I. and K. B. Blodgett, Currents Limited by Space Charge Between Coaxial Cylinders, Phys. Review, Vol. 22, 347-56 (1923).

25. Langmuir, I. and K. B. Blodgett, Currents Limited by Space Charge Between Concentric Spheres, Phys. Review, Vol. 23, 49-59 (1924).

26. Crawford, F. W. and R. Grard, Low-Frequency Impedance Characteristics of a Langmuir Probe in a Plasma, J. Applied Phys., (in press) Jan. (1966).

27. D. B. Beard and F. S. Johnson, Charge and Magnetic Field Interaction with Satellites, J. Geophys. Res., Vol. 65, No. 1, 1-8, (1960).

28. W. W. Zachary, Interim Report on the Plasma Sheath in a Magnetized Plasma, Report NAS-585-5, Electromagnetic Research Corporation, College Park (1962).

29. E. G. Fontheim, W. R. Hoegy, M. Kanal and A. F. Nagy, Theoretical Study of the Moving Langmuir Probe in the Presence of a Magnetic Field, Annual Report No. 1, University of Michigan (1965).

30. F. W. Crawford and S. A. Self, On the Low Pressure Mercury Vapor Discharge Mechanism and the Origins of Langmuir's Paradox, Microwave Laboratory, Stanford University, Rept. No. 1256 (1964).

31. F. W. Crawford, Impedance Characteristics of a Mercury-Vapor Plasma, J. Applied Phys., Vol. 33, No. 1, 20-5 (1962).

32. J. R. Herman, Theoretical Determination of the Impedance Characteristics of a Capacitive Ionosphere Rocket Probe, J. Geophys. Res., Vol. 69, No. 11, 2329-36 (1964).

33. H. B. Palmer, Capacitance of a Parallel Plate Capacitor by the Schwartz-Christoffel Transformation, Trans. Amer. Inst. Elect. Eng., Vol. 56, No. 3, 363-66 (1937).

34. F. E. Terman, Radio Engineers' Handbook, McGraw-Hill Book Co., Inc. (1943).

35. V. P. Pyati and H. Weil, Capacitance of Biconical Antennas in Magneto-Ionic Media; Elliptic Cone Capacitance, Radio Science, Vol. 69D, No. 2, 291-98 (1965).

36. D. Walsh and F. T. Haddock, Antenna Impedance in a Plasma: Problems Relevant to Radio Astronomy Measurements from Space Vehicles, The University of Michigan, Department of Astronomy, Rept. No. 65-9 (1965).

37. F. S. Johnson, Satellite Environment Handbook, Stanford University Press (1965).